Simulation of Severe Thunderstorm Event on 29th April 2019 in Pokhara Using Advance Research Weather Research and Forecasting Model (WRF-ARW)

A Dissertation Submitted to

Central Department of Hydrology and Meteorology, Tribhuvan University

Kirtipur, Kathmandu

As a partial fulfilment for the award of the degree of Masters of Science in Hydrology and Meteorology

Submitted By:

Krishna Ram Prajapati

Symbol No: Hymet110/074

T.U. Regd. No.:5-2-37-120-2012

Central Department of Hydrology and Meteorology

Institute of Science and Technology

Tribhuvan University

Kirtipur, Kathmandu, Nepal

Declaration

I, **Krishna Ram Prajapati**, hereby declare that the dissertation entitled **"Simulation of Severe Thunderstorm Event on 29th April 2019 in Pokhara Using Advance Research Weather Research and Forecasting Model (ARW-WRF) "** presented herein is genuine work, done by myself, and has not been published or submitted elsewhere for the award of any degree. All sources of information have been specifically acknowledged to the author(s) or institution(s) and listed in the references.

…….

Mr. Krishna Ram Prajapati

Central Department of Meteorology and Hydrology

Tribhuvan University

Kirtipur,

Kathmandu

Date:

Letter of Recommendation

This is to recommend that the dissertation entitled **"Simulation of Severe Thunderstorm Event on 29th April 2019 in Pokhara Using Advance Research Weather Research and Forecasting Model (ARW-WRF)"** has been carried out by Mr. Krishna Ram Prajapati for the partial fulfillment of Master's Degree of Science in Hydrology and Meteorology. This is the original work and has been carried out under my supervision. To the best of my knowledge, this thesis work has not been submitted for any other degree in any institutions.

Therefore, I recommend this dissertation for approval and acceptance.

…….

Supervisor

Dr.Dibas Shrestha

Assistant Professor

Central Department of Hydrology and Meteorology

Tribhuvan University

Kirtipur, Kathmandu

Letter of Approval

The dissertation entitled **"Simulation of Severe Thunderstorm Event on 29th April 2019 in Pokhara Using Advance Research Weather Research and Forecasting Model (ARW-WRF)"** by **Mr**. **Krishna Ram Prajapati** has been accepted as a work for partial fulfillment of the requirements for the Master's Degree of Science in Hydrology and Meteorology.

……

Prof. Dr. Deepak Aryal
Head of Department
Central Department of Hydrology and
Meteorology, Tribhuvan University,
Kirtipur, Kathmandu.

Certification

This dissertation submitted by **Mr. Krishna Ram Prajapati** entitled, **"Simulation of Severe Thunderstorm Event on 29th April 2019 in Pokhara Using Advance Research Weather Research and Forecasting Model (ARW-WRF),"** to the Central Department of Hydrology and Meteorology as a partial fulfillment of the requirements for the award of Master's Degree of Science in Hydrology and Meteorology under Tribhuvan University has been accepted and approved by,

…….

Dr.Dibas Shrestha
Assistant Professor
Supervisor
Central Department of Hydrology and Meteorology, Tribhuvan University,
Kirtipur, Kathmandu

…….

Prof. Dr. Sunil Adhakari
External Examiner
Campus Chief
Trichandra Multiple Campus
Ghantaghar, Kathmandu

…….

Mr.NetrajitKhadka
Supervisor
Assistant Professor
Central Department of Hydrology and Meteorology, Tribhuvan University,
Kirtipur, Kathmandu

…….

Dr. Sunil Acharya
Assistant Professor
Internal Examiner
Central Department of Hydrology and Meteorology,
Tribhuvan University,
Kirtipur, Kathmandu

…….

Prof. Dr. Deepak Aryal
Professor (Head of the Department)
Central Department of Hydrology and Meteorology, Tribhuvan University,
Kirtipur, Kathmandu.

Acknowledgements

The journey of this research and my study would not have been possible without the co-operation, warm support and company of many people.

Firstly, I would like to thank my supervisor Dr.Dibas Shrestha for his support, guidance and encouragement from the beginning until the completion of my research. His crucial role to make this report is indescribable. I am thankful to Prof. Dr. Deepak Aryal, Head of Department, for providing me the permission and encouragement to do this research as a partial fulfillment of the requirements for the completion of Master's Degree in Hydrology and Meteorology.

Moreover, I owe my gratitude to co-supervisor sir "Mr. Netra Jit Khadka" who has helped me from the very beginning of my thesis and all the teachers of CDHM. I would also like to thank Mr. Jeevan Bhandari and Mr. Ram Hari Acharya sir for his support and encouragement in doing my thesis.

I am indebted to Mr. Ganesh Kafle, Mr. Kumar Rana, and Mr. Rojan Lamichhane for their help and contributions during my thesis work. I would like to thank my friends and family members who were the constant sources of inspiration of my work without whom this study would have been incomplete.

My Special thanks to The World Academy of Sciences (TWAS) for providing the fellowship to conduct the research with financial as well as technical help.

Lastly, I would like to thank all those who directly or indirectly helped me in the course of study and report preparation.

Krishna Ram Prajapati

2021

Abstract

During the pre-monsoon (March, April and May) in Nepal, severe thunderstorms and hailstorms cause significant property and agricultural damage, in addition to loss of life from lightening. In the present study, Severe thunderstorm event occurred at Pokhara, 800 asl, in Central Nepal on 29th April, 2019, during early afternoon is performed. The event was lasted half hour and produced the golf ball-sized hailstones that destroyed vehicles windshields, damaged the crops worth millions of rupees and more. The Advanced Research-Weather Research and Forecasting (WRF-ARW) model was used to simulate the features associated with a severe thunderstorm and examined its sensitivity to six different micro-physical (MP) schemes (Thompson, Morrison, Goddard, Lin, WSM6 and Ferrier). The three nested domains with the innermost domain of 1km horizontal resolution and integrated for 36hr with the spin-up time of 24 hr. Numerical study of thunderstorms have been discussed with its antecedent thermodynamic stability indices that include K Index, Total totals index (TTI), Convective Available Potential Energy (CAPE), Convective Inhibition Energy (CINE), and Precipitable Water (PW) used for the short range prediction of thunderstorms. For validating simulated features of the thunderstorm, Automatic Weather Station data of Lumle station and observed data of Pokhara synoptic station were used with statistic error analysis using Root Mean Square Error (RMSE), Mean Absolute Error (MAE) and Correlation Coefficient (CC). All the microphysics scheme well predicts the instability indices required for the thunderstorm occurrence. Overall Morrison and Thompson scheme performed well with same correlation coefficient of 0.80, whereas WSM6 has least results with mean correlation coefficient of 0.46 compared to the observed.

Keywords: *WRF-ARW, Microphysics, Thunderstorm, Instability Indices.*

Table of Contents

List of Figures

List of Tables

ABBREVIATIONS

RMSE	Root Mean Square Error
PW	Precipitable Water
NWP	Numerical Weather Predication
NRL	Naval Research Laboratory
NOAA	National Oceanic And Atmospheric Administration
NCEP	National Center For Environmental Prediction
NCAR	National Center For Atmospheric Research
MSE	Mean Absolute Error
MP	Micro-Physics
MMM	Mesoscale And Microscale Meteorology
FAA	Federal Aviation Administration
ESRL	Earth System Research Laboratory
DHM	Department Of Hydrology And Meteorology
CINE	Convective Inhibition Energy
CIN	Convective Inhibition
CC	Correlation Coefficient
CAPE	Convective Available Potential Energy
CAOS	Center For Analysis And Prediction Of Storms
ARW	Advanced Research WRF
AFWA	Air Force Weather Agency
3D	Three Dimensional
TTI	Total Total Index
WRF	Weather Research And Forecasting
WSM6	WRF Single-Moment 6 Class
GrADS	Grid Analysis And Display System

NCEP	National Centers For Environmental Prediction
NCL	NCAR Command Language
NNM	Non-Hydrostatic Mesoscale Model
RIP	Read Interpolate Plot
WPS	WRF Pre-Processing System
VAPOR	Visualization And Analysis Platform For Ocean, Atmosphere, And Solar Researchers
PBL	Planetary Boundary Layer
CCN	Cloud Condensation Nuclei
GFS	Global Forecast System
METAR	Meteorological Aerodrome Reports
UTC	Coordinated Universal Time
JMA	Japan Meteorological Agency
RGB	Red Green And Blue
GDAS	Global Data Assimilation System
READY	Real-Time Environmental Applications And Display System
HYSPLIT	Hybrid Single Particle Lagrangian Integrated Trajectory
ECMWF	European Centre For Medium-Range Weather Forecasts
RRTM	Rapid Radiative Transfer Model
YSU	Yonsei University
KF	Kain–Fritsch
C3S	Copernicus Climate Change Service
ASCII	American Standard Code for Information Interchange
GPM	Global Precipitation Measurement
IMERGE	Integrated Multi-satellite Retrievals for GPM
CTT	Cloud Top Temperature
VT	Vertical Tools

AWS	Automatic Weather Station
SLP	Sea Level Pressure
MSLP	Mean Sea Level Pressure
GRIB	Gridded Binary
NWS	National Weather Service
FNL	Final Operational Global Analysis Data

CHAPTER 1

1 INTRODUCTION

1.1 Background and Motivation

A thunderstorm is a storm with lightning and thunder produced by the cumulonimbus cloud usually accompanied by strong wind, heavy rainfall and sometimes hail. Global statistics of thunderstorms indicate that the most abundant regions of lightning are the tropical continental areas in Africa, South America and Indonesia where thunderstorms occur almost on daily basis (Christian et. Al., 2003). Outside the tropics, thunderstorms have a seasonal cycle which includes Nepal. Nepal is a small country containing complex mountain terrain in north to a tropical low land in the south that lies from 26° 22'N to 30° 27'N in latitude to 80° 40'E to 88° 12'E in longitude. Within an east west distance of less than 1000 km and north south distance of about 200km there exist a altitudinal gradient from 59 m.a.s.l in the southern Terai to Highest peak 8848 m.a.s.l in the northern Himalayan range. Physiographicaly Nepal is divided into five regions Terai, Siwaliks, Middle Mounatins, High Mountains and High Himalayas (Kansakar et al., 2004). These physiographical and topographic extremes present in Nepal are the cause for the presence of multiple climate variation in the country. Almost all types of climates, subtropical to alpine climate are found in Nepal. The climate of Nepal is mainly characterized by altitude, topography and seasonal atmospheric circulation. As the occurrence of monsoon rains is dominant in the temporal distribution of pre-monsoon, the season can be defines as: monsoon (June to September), post-monsoon (October to November), winter (December to February), and pre-monsoon (March to May) in Nepal("Report: Study of Climate and Climatic Variation over Nepal," 2015). During the summer monsoon large amounts of moisture and precipitation are brought form the Indian Ocean to Nepal which is the cause for the flood and landslide in Nepal (Robinson and Henderson-Sellers, 1999; Malla, 2008). And before the monsoon (pre-monsoon), the atmosphere changes into highly unstable and intense convection which is the causes for the occurrence of thunderstorms. This pre-monsoon season is the most lightning abundant period in Nepal and it has also been noted to reach extreme intensity and have a great impact to the countries (Makela et al., 2012).

Nepal is one of the most weather related disaster-prone countries in the world. The various types of weather and climate related disasters are floods and landslides, thunderstorm, droughts, storms, avalanches, hailstorms etc. Table1.1 clearly shows that thunderstorm claim large number of human life and the number of thunderstorm is increasing. On the year 2019, the death caused by the thunderstorm is more than any other disaster in Nepal.

Table 1.1 Year wise disaster scenario loss of lives and major types of disaster in Nepal form 2000 to 2019.

Year	Fire	Flood and Landslide	Thunderbolt
2000	53	173	23
2001	26	196	39
2002	14	441	3
2003	16	232	42
2004	10	131	10
2005	27	141	18
2006	28	141	17
2007	34	216	35
2008	11	134	14
2009	35	135	7
2010	42	240	39
2011	46	263	95
2012	77	123	119
2013	59	219	146
2014	62	241	96
2016/15	104	377	185
2018/17	150	344	160
2019	78	159	94

(Source : Nepal disaster report; http://drrportal.gov.np/)

On 29th April 2019, golf-ball-sized monster hail inflicted heavy damage to crops in Pokhara, Nepal (https://thehimalayantimes.com/nepal/hailstorm-destroy-property-worth-millions-in-pokhara). Within 30 minutes the hailstorm rampage has damaged the crops, worth millions of rupees, destroyed vehicles windshields. The major cities where downpour inflicted heavy damage to crops are Kaskikot, Dhikurpokhari, Bhadauri, Sarangkot, Pumdibhumdi, Hemja, Malepatan, Masbar, Pasang, Charepatan, Kristi, Lamachaur, Dhumpus, Dhital in the district. According to Manohar Kadariya, Chief of

Agriculture Department in Pokhara Metropolitan City, hailstorm destroyed both seasonal and off-season crops and fruits in the region.

Numerical Weather Prediction (NWP) has been more reliable and precise system for weather forecasting in the recent decades. Identification of the severe events and its possible impacts is very important for the reduction of the risk. The high resolution regional model also known as convection permitting models have been used for the early detection of the severe weather events. (https://www.wmo.int/pages/prog/www/swfdp/Meetings/documents/Advances_NWP.pdf). Advancement in numerical models with data assimilation technique has shown better results in forecasting rainfall (Kumar et al., 2016; Rakesh et al., 2009). Disaster management requires proper information for preparedness and mitigation. Global and regional models can be a promising tool to make community better prepare for the upcoming weather related challenges.

1.2 Rational of Study

Thunderstorm is one of the most devastating, yet spectacular weather phenomena that cause mass destruction to properties and lives. Thunderstorm are very common and is one of the most devastating hazards in Nepal because of a large amount of atmospheric water vapour coming from the Indian Ocean and a large orographic lifting of this moist air. In 2019, a total of 2884 people were affected by lightening, with loss of USD 110,982 and the fatality number was the highest (94) in reported lightning events since 1971(Adhikari, 2021). Even though thunderstorms have deadest effect on human life and properties damages, there has been very few research on this field. There is no sufficient and satisfactory data recorded for the proper study of the thunderstorm. Forecasting of the severity of thunderstorms requires meteorological infrastructure and resources and Thunderstorm intensity has been always difficult to forecast (Carlson and Ludlum., 1968). But there is lack of resource in Nepal. So, for the improvement of the prediction and for the understanding the thunderstorm features, studying thunderstorm using of the WRF model can be one of the important tool.

1.3 Study Area

Pokhara is the headquarter of Gandaki Provience and lies in the Kaski district of Nepal. The latitude and longitude of Kaski district is 28°18′19.08″ North and 84°04′37.20″ East. The Kaski district consist of diverse topography including mountains, hills and valleys that ranges from 450 meters the lowest land to 8091 meters the highest point in the

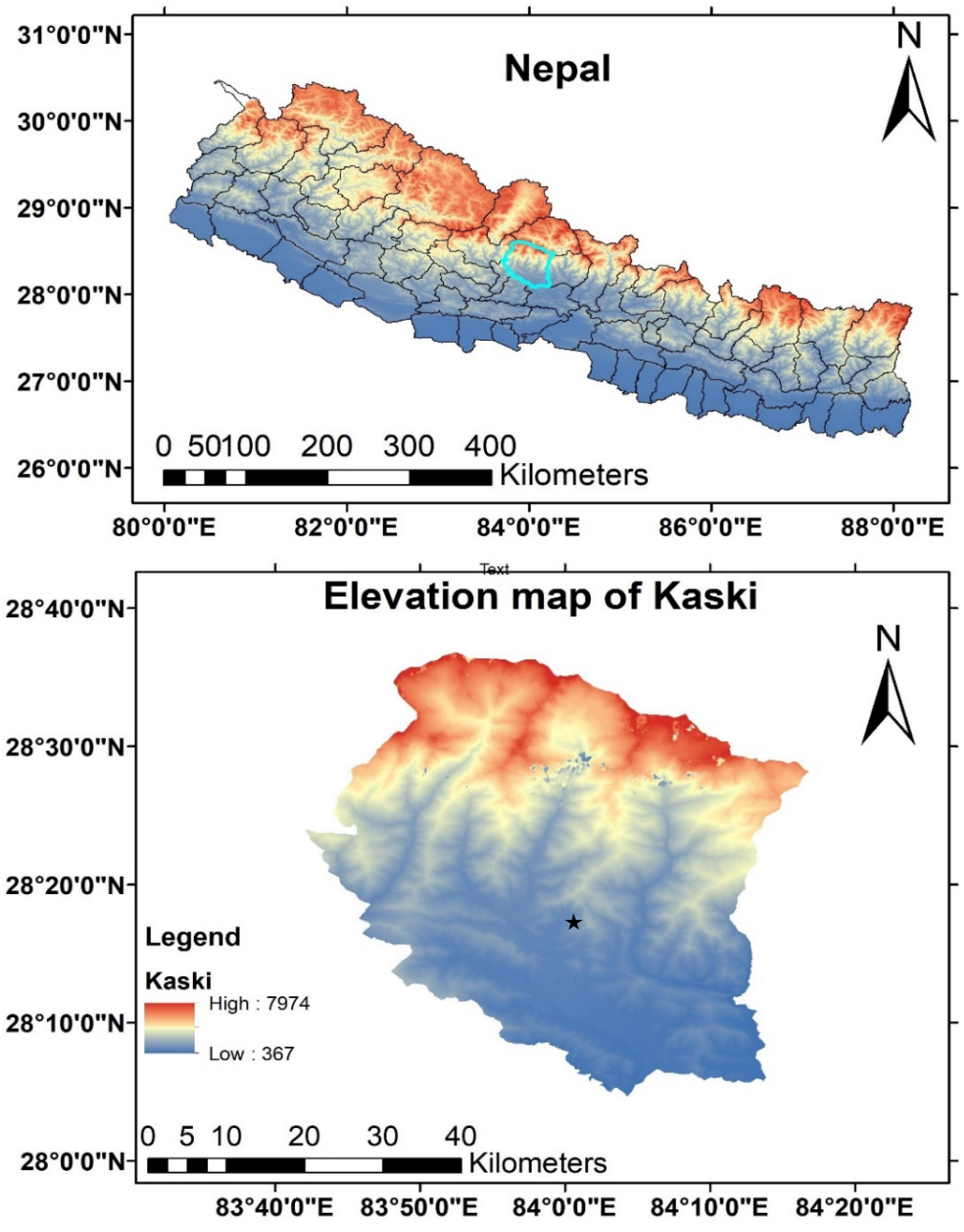

Figure 1.1 Map of Kaski district Nepal. Blue line represent Kaski district and black star represent Pokhara station.

Himalaya range.

Pokhara (800m) also known as the "City of the Lake" is one of the wetland type valley that lies in the region of the Himalayas where often severe weather like heavy precipitation, shower, hailstorm and thunderstorm occurs. Pokhara is one of the main rain pocket area of Nepal. It is surrounded in the east, north and northwest by high mountains. These act as barriers and induce precipitation from orographically lifted humid air. Precipitation results also from mountain-valley flows that are drawn into the area each day. These features explain why Pokhara is a moisture convergence zone that receives some of the highest precipitation in Nepal.

1.4 Research Questions

This study is based on the study of thunderstorm in Pokhara on 29th April 2019. This event was interesting since its phenomenon occurred only for around 30 minutes delivering many damages. To provide more insight on this event, following research questions are formulated.

- How reliable WRF model to simulate the thunderstorm event on 29th April 2019?
- Which microphysics scheme lead to the best performance in the study?

1.5 Objectives of Study

The main objective of the study is to simulate the severe thunderstorm and its structure at finer resolution to understand the extreme thunderstorm events using the WRF model. The vision of the study is to improve the prediction of this important weather phenomenon. For this, analysis of the distribution of extreme thunderstorm during Pre-Monsoon is important as Pre-monsoon is the season of thunderstorm. The specific objectives of the study are:

- To simulate the WRF microphysics scheme for studying the characteristic of the thunderstorm.
- To analysis the extreme thunderstorm events.
- To identify the best scheme for the study of thunderstorm.

CHAPTER 2

2 LITERATURE REVIEW

2.1 Pre Monsoon Thunderstorm in Nepal

The Earth's atmosphere is majestic in its beauty, awesome in its power and complex in its behaviour. The thunderstorm resulting from vigorous convective activity, is one of the most devastating, yet spectacular, weather phenomena (Rahman et al., 2018).The foothills of Himalaya (Saha et al., 2019), eastern and north-eastern part of India (Das et al.,2014), Bhutan, Bangladesh(Yamane et al., 2010) experience frequent thunderstorms during premonsoon season due to variation of surface temperature, wind speed and moisture inflow from bay of Bengal. The study conducted by (Manohar and Kesarkar, 2005) shows that India experiences about 56% of total annual thunderstorms in monsoon season and about 30% of it in pre –monsoon season. On yearly basis, the eastern and northeastern part of India is more vulnerable to thunderstorm than the remaining part. Thunderstorm climatology of Bangladesh (Islam et al., 2020) shows that on monthly basis on may and on seasonal basis monsoon has the highest thunderstorm frequency. However the lightening climatology (Dewan et al., 2018) shows greater lightening distribution of 69.2% in pre-monsoon and 24.1% in monsoon and remaining about 7% in winter and post monsoon indicating more convective activity during pre-monsoon season. The lightening activity is found to be high in evening during pre-monsoon and in early morning and evening during monsoon seasons.

In context of Nepal, pre-monsoon season (April, May and June) is the most lightning abundant period in Nepal and it have also been noted to reach extreme intensity and have a great impact to the countries (Mäkelä et al., 2012).The statistics shows higher thunderstorm activity during pre-monsoon (43%) with peak activity in april and may(Saha et al., 2019) than in monsoon (36%) but the diurnal distribution of lightening activity showed similar peak at early evening (Mäkelä et al., 2014). During the pre-monsoon months, a series of slow building thermally induced surface or heat lows begin establishing in the northwest corner of India and Pakistan (Panta et., al., 1997, Rao 1981). During this pre-monsoon period the intense heating of land result in the formation of permanently thermally induced low in the north-western part of the subcontinent. The sub-tropical surface heat lows can manifest themselves up to the 700hPa level, but do not generate convective activity unless the appropriate synoptic condition are present. The

primary surface heat low is located in the semi-arid regions of northwest India; a secondary heat low develops south of Nepal, over the North Indian plains (Aryal, 2018). During April and May, the secondary heat low is not a stationary phenomenon and tends to change its location.

Convective activities are more pronounce in pre-monsoon period in the country like Nepal. Most of the thunderstorm activities are occurs in afternoon. During the establishing of the monsoon trough when all southwest monsoon pre-requisites are falling into place, the northeast corner of the Indian subcontinent is characterized by vigorous thunderstorm activity (Rao 1981, Pant and Rupa 1997, Laing and Fritsch 2007, Mandhar et. al., 1999). Several areas are particularly susceptible to violent weather. These include North East India, Bhutan, Bangladesh, and the foothills of the Himalayan Range in Nepal. Colder than normal temperatures from a continuous succession of mid-tropospheric waves, “Western Disturbances", sweep across the northern Indian subcontinent with the still very active sub-tropical jet stream.

The number of severe and extreme thunderstorm events are increasing every year (Makela et al., 2012). According to (Diffenbaugh et al., 2008; Seeley and Romps, 2015) the severe thunderstorm forcing is likely to increase due to higher concentration of GHG’s. On 31 March 2019, a powerful windstorm liquidated two districts (Bara and Parsa) of southern Nepal with heavy rainfall, thunderstorm, hail and destructive wind storm. Department of Hydrology and Meteorology listed it as the first documented Tornado in Nepal. Meyer et al., (2021) Simulated the Tornado event indicate that such extreme severe weather, while rare, have the potential to be anticipated in the future.

Inhabitants of Nepal’s rural areas have become accustomed to almost daily thunderstorms during the month of May (Makela et al., 2013), with accompanying lightening and often hail. Saha et al.,(2019) analyzed lightening climatology over Nepal for first time on the base of Satellite data. They found that the months of April and May are extremely vulnerable in the perspective of lightening hazards in Nepal, in contrast to the results reported previously which indicated that the maximum lightening activity occurred in the month of June. It was also found that the central and eastern regions of the country receive the majority of lightning strikes during the months of April and May. In long-term analysis of lightning fatalities and injuries in Nepal. Adhikari, (2021) shows that the overall countrywide lightning fatality rate of the entire period is 1.77 per million per year.

It was also concluded that the increase in lightning fatality events in recent years is due to internet penetration and the high and low concentrations of loss and damage are mainly due to geographic distribution, population density, and economic activities and recommends the establishment of lightning early warning systems in Nepal. But forecasting the severity of thunderstorms requires advance technology which Nepal simply does not have. Carlson and Ludlum, (1968) found that the study of Thunderstorm intensity is always difficult to forecast even in highly developed and industrialized counties around the world where weather forecasters with Doppler radar, portable radiosonde equipment and unlimited computer power are easily available.

2.2 WRF in Study of Thunderstorm

Forecasting thunderstorms is one of the most difficult tasks in weather prediction, due to their rather small spatial and temporal extension and the inherent non-linearity of their dynamics and physics. The use of Numerical Weather Prediction (NWP) system to complement the interpretation of conventional observations added great value to TS forecasting (Ahasan et al., 2015). Weather Research and Forecasting Model is widely used Numerical model for both the research and forecasting. It has been used extensively to study severe thunderstorms, precipitation, windstorm, hurricane, drought, pollution and many more. WRF model is able to simulate the spatiotemporal distribution of mesoscale phenomenon arising in the Himalayan region but the study is limited to few numbers (Karki et al., 2018; Norris et al., 2015; Maharjanand Regmi, 2015; Shrestha et al., 2017) in context of Nepal. Few experiments using NWP model have been done for high impact weather events over the different regions of Nepal. Karki et al., (2018) studied about simulation of an extreme precipitation event over the Central Himalayas using WRF model to find out the atmospheric mechanisms and their representation. Similarly, Shrestha et al., (2017) done the sensitivity test of different WRF cloud microphysics of a Convective Storm over the Nepal. Orr et al., (2017) also studied the sensitivity of summer monsoonal precipitation in Langtang valley of central Himalaya using WRF model.

Papa Rao G, (2016) use the WRF-ARW model for the prediction study of severe thunderstorm over Siharikota with two nested domain of 27km and 9km resolution. With simulation of three case study it was concluded that the model was able to predict thunderstorm well but suggested for more study with better resolutions. Paul et al., (2019)

study pre-monsoon thunderstorm with two event on 19th April 2018 over Chattogram and 4th May 2018 over Dhaka for which different stability indices were investigated.

Mannan et al., (2015) diagnosethe severe thunderstorm event over Bangladesh with six different microphysics scheme and four cloud physics scheme to find the best combination. Similarly sensitivity experiment of WRF cloud microphysics for the simulation of convective storm over Nepal Himalayas was performed (Rajeevan et al., 2010) with an aim to investigate microphysical dependence of simulated characteristics of a convective storm that generally develops during the pre-monsoon season over the foothills of the Himalayas. The results show that reasonably well with the observations across Siwalik Hills and Middle Mountains, which act as a topographic barrier for low level circulation and significantly influence formation and distribution of rainfall, receives more rain but show negative bias across central Nepal including the Kathmandu Valley.

Singh et al., (2017) have studied the severe thunderstorm in Indian subcontinent and examined the sensitivity of domain resolution on model performance. The simulation predicts better results with 1 km grid resolution compared to 9 km and 3 km grid resolution results.

Bonekamp et al., (2018) found the simulations are also sensitive to the spin-up time (especially in the summer period), without a clear trend with increasing length. They found a spin-up time of 24 h gave the highest correlations of precipitation, 2-m air temperature, and 10-m wind speed compared to the periods of 12 h, 3 days, and 5 days. Furthermore, they suggest that future modelling studies of High Mountain Asia should consider a sub kilometer grid for accurately estimating local meteorological variability.

Meyer et al., (2021) simulate the storm environment responsible for Nepal's first observed Tornado recorded on 31st March 2019.The study was carried out with multifaced view of the storm environment through a synoptic perspective provided by GDAS reanalysis dataset and a trio of pregressively higher resolution one-way nested simulations. WRF model was used for simulating the pre-storm mesocale environment and thermodynamic environment and also simulated the convective indices. (Chhetri et al., 2019) have carried out the study of First Tornado Nepal (FTN) suggest that the large instability of the atmospheric condition with large heating system of surface temperature and solar radiation with the two systems of air mass (Westerly and S-Easterly) transports

combined each other and produced the environment for the formation of more powerful tornado on 31 March 2019 in Nepal.

Investigation of severe thunderstorm with hailstorm indicated that WRF-ARW could simulate thunderstorm with hail well under synoptically favourable conditions, although there is some space-time error (Chevuturi et al., 2014; Murthy et al., 2018).The effect of different microphysics scheme on WRF-ARW model was studied with a case study of hailstorm in Surabaya, Indonesia (Sari et al., 2018). It was found that the Thompson scheme was more suitable to reproduce cloud convection and able to generate cloud properties in proper condition when hail event is possible to occur.

CHAPTER 3

3 DATA AND METHODOLOGY

3.1 Data

Different data set like in-situ, satellite data and climatic model data are use in the study. The data sets used in the study are as follows:

3.1.1 Initial and Lateral Boundary Conditions

The global six hourly datasets from National Centers for Environmental Prediction (NCEP) Global Forecast System (GFS) obtained from the Research Data Archive of NCAR/UCAR (https://rda.ucar.edu/datasets/ds083.2/) have been used to provide the initial and lateral boundary conditions for WRF model at $1^0 \times 1^0$ grid resolutions. The datasets have the temporal resolution of 6 hour. The analyses are available on the surface, at 26 mandatory (and other pressure) levels from 1000 millibars to 10 millibars, in the surface boundary layer and at some sigma layers, the tropopause and a few others. Parameters include surface pressure, sea level pressure, geopotential height, temperature, sea surface temperature, soil values, ice cover, relative humidity, u- and v- winds, vertical motion, vorticity and ozone.

3.1.2 In-Situ Observation

Department of Hydrology and Meteorology (DHM) is the official body of Nepal Government that provides the hydro-meteorological data for the study. Out of the 16 synoptic station present in Nepal, one of the station is Pokhara station which lies in the study area. The synoptic data recorded every three hour from this station was used which include surface temperature, wet bulb and dry bulb temperature, due point temperature, humidity, past and present weather, mean sea level pressure. Beside that from 00 UTC to 12 UTC METAR data were also recorded every hour which include mean sea level pressure, air temperature, visibility, dew point temperature, cloud amount and type. Precipitation data AWS in Lumle was used for model verification.

3.1.3 Satellite Image

The Himawari satellite is a geostationary satellite, operated by the Japan Meteorological Agency (JMA) that provides free access to download the images (https://www.data.jma.go.jp/mscweb/data/himawari/sat_img.php?area=se4).

Meteorological Satellite Center of JMA provides the satellite imageries in different band such as B13 (infrared), B03 (visible), B08 (water vapour), B07 (shortwave infrared), dust RGB, airmass RGB, True colour RGB and many other. It supports in weather forecasting, tropical cyclone tracking, and meteorology research. Apart from the Japan many meteorological agencies in East Asia, Southeast Asia, Australia, New Zealand and Nepal use the satellites for their own weather monitoring and forecasting operations.

3.1.4 GDAS Data

The Global Data Assimilation System (GDAS) is the system used by model to place observations into a gridded model space for the purpose of starting weather forecasts with observed data. GDAS use 3-D, model space: surface observations, balloon data, wind profiler data, aircraft reports, buoy observations, radar observations and satellite observations to a gridded format. In the research, a GDAS datasets available at 1^0 resolution is use through HYSPLIT (Hybrid single Particle Lagrangian Integrated Trajectory) model. HYSPLIT model is complete system for computing air parcel trajectories, transport, deposition and dispersion of atmospheric pollutants. It is designed for quick response to atmospheric emergencies, diagnostic case studies or climatological analysis using previously gridded meteorological data. It can be run interactively on the READY web site (http://ready.arl.noaa.gov/HYSPLIT.php).

3.1.5 Reanalysis Datasets

To analyse the synoptic environment characteristics and validate with the WRF output the ERA5 datasets is use in the study. ERA5 is the fifth generation ECMWF reanalysis datasets for the global climate and weather provided by European Center for Medium-Range Weather Forecasts (ECMWF). Reanalysis combines model data with observations from across the world into a globally complete and consistent dataset using the laws of physics. It provides global gridded data at the horizontal resolution of 0.25×0.25^0. The vertical resolution includes data for 37 pressure levels from surface to the height of 1 hPa. ERA5 provides hourly estimates for a large number of atmospheric, ocean-wave and land-surface quantities in GRIB format. ERA5 is updated daily with a latency of about 5 days. ERA5 hourly data on pressure levels can be freely downloaded from Copernicus Climate Change Service (C3S) Climate Data Store.

https://cds.climate.copernicus.eu/#!/search?text=ERA5&type=dataset

3.2 WRF Modelling System

The following figure shows the flowchart for the WRF Modelin

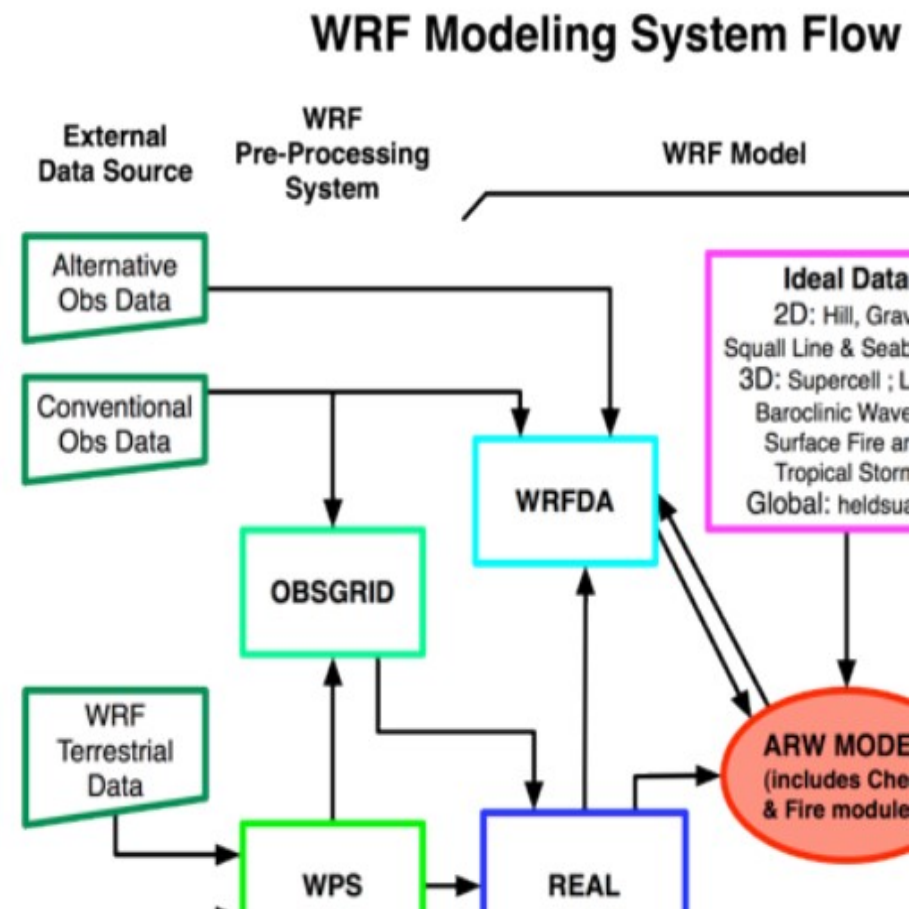

Figure 3.1. Data flow among programs in WRF Preprocessing System (Skamarock et al., 2008)

The Weather Research and Forecasting (WRF) model is a next-generation mesoscale numerical weather prediction system designed for atmospheric research and operational forecasting applications. This model is the result of a collaborative effort between the National Center for Atmospheric Research's (NCAR), Mesoscale and Microscale Meteorology (MMM) Division, The National Oceanic and Atmospheric Administration's (NOAA), National Center for Environmental Prediction (NCEP) and Earth System Research Laboratory (ESRL), The Department of Defence's Air Force Weather Agency (AFWA) and Naval Research Laboratory (NRL), the Center for Analysis and Prediction of Storms (CAOS) at the University of Oklahoma and the Federal Aviation Administration (FAA) with the participation of university scientist (Skamarock et al., 2008). It is community based model that is freely available internationally for research,

operational and teaching. It have wide range of applications in Atmospheric physics research, case study research, real time NWP and forecast system research and more.

The WRF Modeling System consists these major programs: WRF Pre-processing system, WRF model and Post-processing and visualization.

WRF Pre-processing System (WPS): The WRF Preprocessing System is a set of programs that prepares input data for WRF model. The purpose of WPS is to define simulation coarse domain and nested domains, computes latitude, longitude, map scale factors and coriolis parameters at every grid point. It is also use to interpolate time-invariant terrestrial data to simulate grid and to interpolate time-varying meteorological fields from another model onto simulation domains. WPS is further divided into three major programs. The static fields and grid domains are specified in the first program, ***geogrid***. The external analysis and forecast data are decoded from the Grib format with the ***ungrid*** program in WPS. The final program in the WPS suite is the ***metgrid*** program, which horizontally interpolates the data from ungrid.

WRF Model: WRF model have two cores of dynamic solvers for its computation of the atmospheric governing equation and the variants of the model. Advance Research WRF (ARW) solver developed by NCAR (Skamarock, 2005) is a fully compressible, Eulerian non-hydrostatic model with a run-time hydrostatic option available and the Non-hydrostatic Mesoscale Model(NNM) solver developed by NCEP (Janjic, 2003) is a compressible hydrostatic NWP model using mass based vertical coordinate, which have been extended to include the non-hydrostatic motions.

The ARW system consist of fully compressible non-hydrostatic equations with different prognostic variables. There is option for user-defined domains and for downscale coarse resolution to fine resolution by using nesting capability in the model. Nesting can set as either two-way, one-way or with a moving nest model for different kind of atmospheric simulations. The WRF-ARW dynamical core is primarily responsible for vertical coordinates, horizontal grid, time integration, terrain representation, prognostic equations, variables, grid staggering, advection, boundary conditions, nesting, map projections, filters, time step and nudging. It can be run on wide range of computer systems from single-processor computer to large server systems which has shared memory distributed-memory with a high level of computational power.

Post-processing & Visualization tools:

Several programs are there for data processing and visualization of WRF output. NCAR command Language (NCL) developed by the Computational and Information Systems Laboratory at the National Centre for Atmospheric Research is the free interpretable language for designing, processing and visualization of scientific data. ARW post is a FORTRAN based program that reads WRF-ARW output files and then create files readable by GrADS (Grid Analysis and Display System). Similarly, RIP (Read Interpolate Plot) is a Fortran program that utilizes the NCAR Graphics System Plot Package. It is more suitable for creating plots, primarily from mesoscale model output. There are also Program VAPOR (Visualization and Analysis Platform for Ocean, Atmosphere, and Solar Researchers) developed by VAPOR team and NCAR that is the 3-dimensional data visualization tool.

WRF-ARW Physical Parameterization

Models cannot resolve local flows, swirls, obstacles and microscale phenomena existing

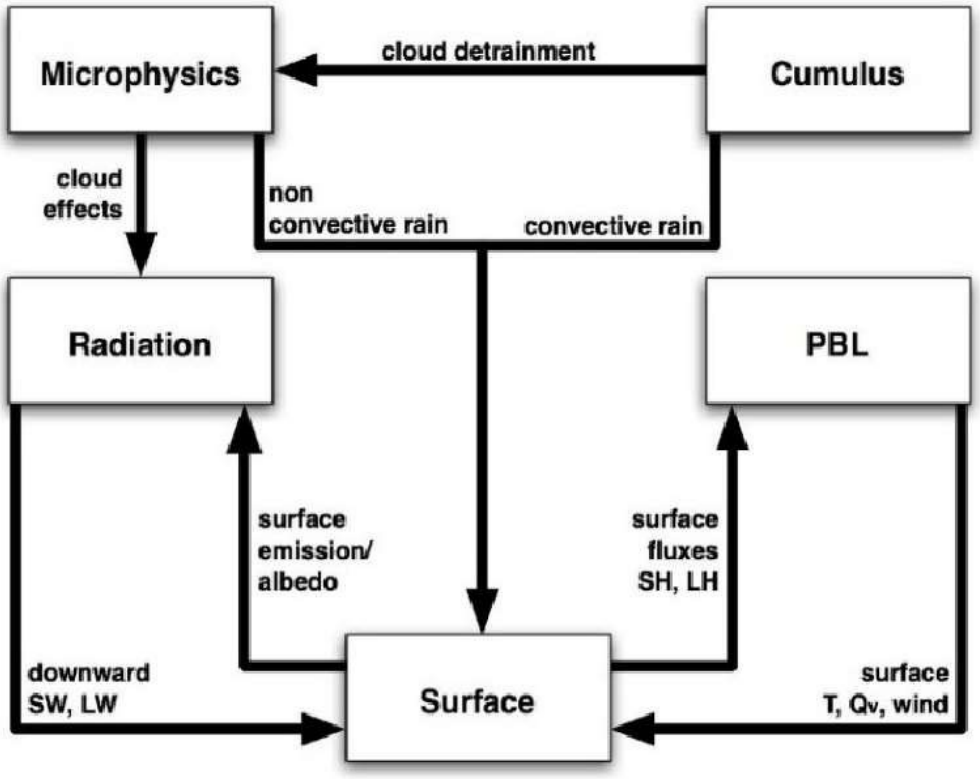

Figure 3.2. Interactions among the five major physical parameterization in the WRF-ARW (Skamarock et al., 2019)

within the grid box. A procedure to represent these process by relating them to variables on the scales that model resolves are called parameterizations. Knievel (2007) defines physical parameterization in WRF as the one that approximate the bulk effects of physical processes too small, too brief, too complex, too poorly understood, or too computationally costly to be explicitly represented. The physical and dynamical processes are represented by several equations. Equations representing these processes ranges from simple to complex. Computers are not yet powerful to calculate each complex process explicitly because either they are too small or too complex to resolve explicitly or some are not sufficiently understood to represent in equation format. Hence, parameterization is account for smaller than grid size physical processes that can't be explicitly resolved (without parameterization) by the dynamical core of WRF-ARW (Skamarocket at., 2008).

Various physical parameterization schemes have been developed with the development of advanced computing system and high resolution models (Figure 2.2). The physics option are Microphysics, Cumulus parameterization, Radiation, PBL, Land Surface model, Turbulence and Diffusion. Cumulus parameterization are responsible for sub-grid scale effects of convection and shallow cloud. Cumulus schemes are intended in the model to represent vertical fluxed due to unresolved updrafts and downdrafts and compensating motion outside the clouds. The planetary boundary layer physics is responsible for vertical sub-grid-scale fluxed due to eddy transports in the whole atmospheric column, not just the boundary layer it determines the flux profiles within the well-mixed boundary layer and the stable layer. The radiation schemes provide atmospheric heating due to radiative flux divergence and surface downward longwave and shortwave radiation for the ground heat budget. Longwave radiation includes infrared or thermal radiation absorbed and emitted by gases and surfaces. Upward long wave radiative flux from the ground is determined by the surface emissivity that in turn depends upon land-use type, as well as the ground temperature. The land-surface models use atmospheric information from the surface layer scheme, radiative forcing from the radiation scheme, and precipitation forcing from the microphysics and convective schemes, together with internal information on the land's state variables and land-surface properties, to provide heat and moisture fluxes over land points and sea ice points which in turn provide a lower boundary condition for the vertical transport done in the PBL schemes.

Microphysics includes explicitly resolved water vapor, cloud, and precipitation processes. It describes the inter conversion of moisture to precipitation and vice versa. The impact of

cloud microphysics on cloud resolving simulations is an important issue in NWP and regional climate modelling. The selection of microphysical parameterization is always crucial for prediction of precipitation (Michael Fritsch and Carbone, 2004). Some of the microphysics schemes that is used in this study are WSM6-class scheme (Hong and Lim, 2006), Morrison 2-moment scheme (Morrison et al., 2009), Perdue Lin scheme (Lin et al., 1983), Goddard scheme (Tao et al., 1989), and Thompson 6-class microphysics scheme with graupel (Thompson et al., 2008).

WSM6-class scheme: WRF Single-Moment 6-class (WSM6) scheme is most suitable for cloud resolving grids. It also consists of six hydrometeors: water vapor, cloud water, rain, cloud ice, snow and graupel to resolve water vapor, cloud and precipitation processes. A new method for representing mixed-phase particle fall speeds for the snow and graupel by assigning a single fall speed to both that is weighted by the mixing ratios and applying that fall speed to both sedimentation and accumulation processes in introduced (Dudhia, Hong and Lim, 2008). It is single moment scheme and mostly used for high resolution simulation.

Lin scheme: Lin scheme includes six classes of hydrometeors: water vapour, cloud water, rain, cloud ice, snow and graupel. This is a sophisticated microphysics scheme in WRF, and it is most suitable for use in research studies.

Goddard scheme: This is a single-moment 6-class microphysics scheme [Tao et al., 2009]. This includes cold rain processes defined by Rutledge and Hobbs [1984] and Mc. Cumber et al. [1991]. Tao et al. [1989] added several saturation techniques, a new process for the conversion of cloud ice to snow, and corrections regarding graupel-related variables following the specifications of Braun and Tao [2000] and Lang et al. [2007].

Thompson scheme: It is a single-moment scheme, although for cloud ice and rain it also acts as a double-moment scheme. The Thompson scheme determines the hydrometeor mixing ratio and, for rain and cloud ice hydrometeors, also the number concentration. Snow shape is considered non-spherical, with bulk density varying inversely with diameter as in observations [Thompson et al., 2004], and its size distribution is represented as a sum of exponential and gamma distributions.

Morrison 6-class double-moment scheme: Morrison 2-moment scheme involves the development of graupel in generation of precipitation. In this scheme number

concentrations are also predicted for ice, snow, rain and graupel. It includes more complicated microphysics, estimating number concentrations and mixing ratios of four hydrometeor species (cloud water, cloud ice, rainwater, and snow), rain size distribution, and different rates of rain evaporation in stratiform and convective regions. Cloud number concentration is diagnosed. The Morrison microphysical parameterization has options to optimize simulations by accommodating the selection of ice nucleation method and CCN spectra [Morrison et al., 2005].

Ferrier scheme (Ferrier, 1994)**:** Ferrier scheme is also double moment, 4-class ice-phase microphysics scheme. It consists of 90 microphysical processes that has improved parameterization of several cloud and precipitation processes. It is designed with combine features from Lin et al. 1983, Rutledge and Hobbs 1984, and other for efficiency diagnostic cloud water, rain and ice(cloud ice, graupel) form storage arrays.

3.3 WRF-ARW Model Setup

The Advanced Research Weather Research and Forecasting (WRF-ARW) model version

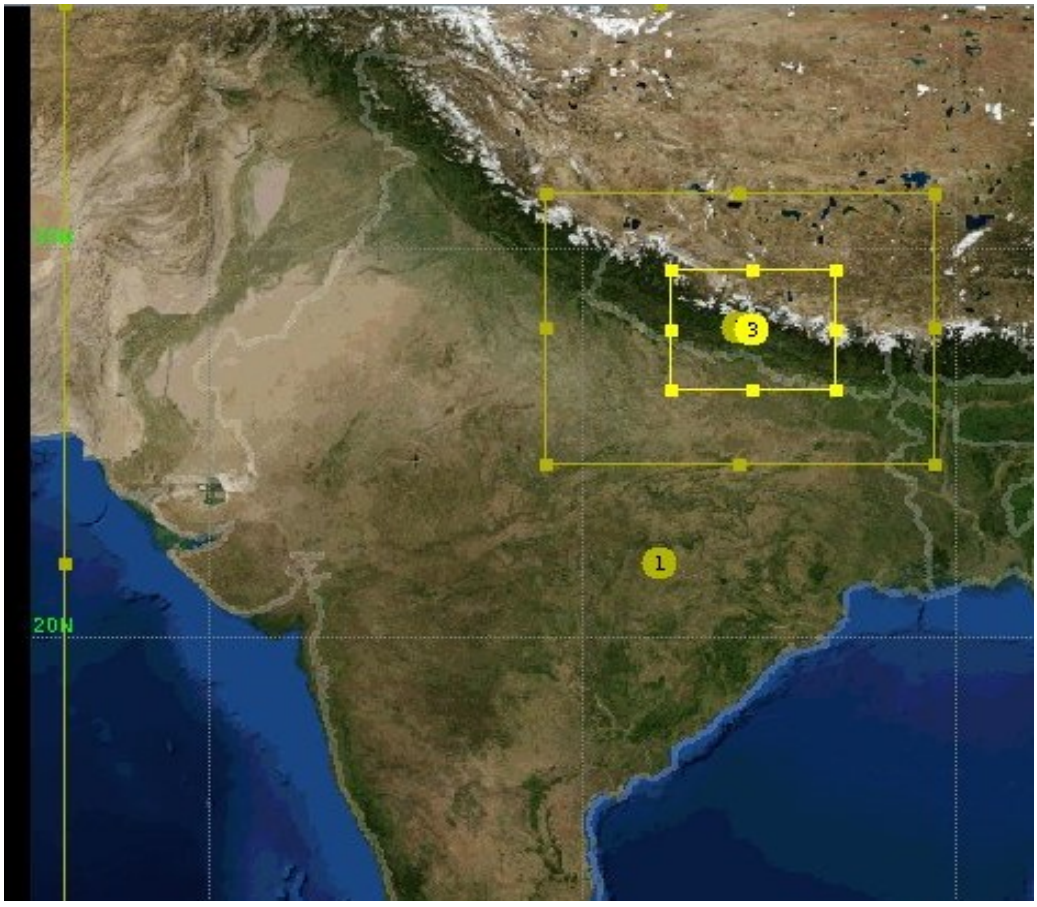

Figure 3.3 Nested WRF Domain

4.0.3 is used for the simulation of the event. The Weather Research and Forecasting (WRF) is a fully compressible, three-dimensional (3D), eulerian, non-hydrostatic, primitive-equation regional atmospheric model with multiple nesting abilities (Skamarock et al., 2019). It is available with several advanced physics and numerical schemes, designed for better prediction of atmospheric processes and operational forecasting.

The model is Initialized at 1200 UTC 28th April 2019 and integrated until 0000 UTC 29th April 2019 (36 hours). The first 24 hours (around) of simulation is regarded as spin period. The three nested domains with horizontal grid resolutions of 25km, 5km and 1km Mercator projection are designed with 40 verticals sigma levels. The initial and lateral boundary are used form 6-hourly FNL Global Analysis at $1^0 \times 1^0$ grid resolution. A detail about configuration of the model setup is given in Table 3.1.

Table 3.1 Model configuration and design.

Model options	**Dataset or value**	
Model	WRF-ARW version 4.0.3	
Domains	3	
Grid resolution (spacing)	25, 5 and 1km	
Downscaling ratio	1:5	
Projection system	Mercator	
Microphysics schemes	1. Lin	4.Thompson
	2. Eta (Ferrier)	5. Goddard
	3. WSM6	6. Morrison
Initial conditions	NCEP FNL at $1^0 \times 1^0$ grid	
Shortwave radiation scheme	Dudhia	
Longwave radiation scheme	Rapid Radiative Transfer Model (RRTM)	
PBL Schemes	Yonsei University (YSU)	
Cumulus schemes	Kain–Fritsch (KF)	

3.4 Data Visualization

WRF-ARW model data can be visualized through number of visualization tools. Some visualization tool used during the research is described below:

NCAR Command Language (NCL)

NCL is an open source interpreted language. It is usually designed for the analysis and the visualization of the scientific data. It supports numerous input file formats: netCDF3, netCDF4, GRIB1, GRIB2, HDF-SDS, HDF-EOS, HDF5, Fortran/C binary, shape files and ASCII. NCL can be run in interactive mode or the batch mode. For the research NCL version 6.6.2 is used.

Python

Python is the popular programming language. It has wide range of application and offers multiple great graphing libraries that come packed with lots of different features. Calculation.

3.5 Statistical Error Analysis Method

Verifying the simulated model results measures how the values of the forecasts differ from the values of the observations. For this point data are compared with the AWS data and observed data provided by DHM as per the data available. The parameters used in the validation are sea level pressure, air temperature and precipitation. The following statistical parameters were calculated for the comparisons between the model output and observation data.

Mean Absolute Error (MAE): This is the average over the verification sample of the absolute values of the differences between forecast and the corresponding observation. The MAE is a linear score which means that all the individual differences are weighted equally in the average. The MAE is a common measure of forecast error in time series analysis. It measures accuracy (the level of agreement between the forecast and the observations) for continuous variables. The MAE is given by Equation

$$\boldsymbol{MAE = \frac{1}{N}\sum_{i=1}^{N} |Mi - Oi|}$$

Where Mi is the model output and Oi is the observation. The difference between the model and the observation is the error. The lower the errors, the greater the accuracy. The range is 0 to infinity. The perfect score is 0.

Root Mean Square Error (RMSE): Root Mean Square Error is a frequently used measure of the differences between values predicted by a model and the values actually observed. It measures average error, weighted according to the square of the error. It does not indicate the direction of the deviation. The RMSE puts greater influence on large errors than smaller errors, which may be a good thing if large errors are especially undesirable, but may also conservative forecasting. The RMSE is given by

$$\boldsymbol{RMSE} = \sqrt{\frac{\mathbf{1}}{\boldsymbol{N}}\sum_{\boldsymbol{i=1}}^{\boldsymbol{N}}(\boldsymbol{Mi}-\boldsymbol{Oi})^{\mathbf{2}}}$$

Correlation Coefficient: This indicates the strength and direction of a linear relationship between two random variables. That means it measures the strength of the linear relationship between the forecasts and observations. The *r* is given by

$$\boldsymbol{r} = \frac{\sum(\boldsymbol{M}-\bar{\boldsymbol{M}})(\boldsymbol{O}-\bar{\boldsymbol{O}})}{\sqrt{\sum(\boldsymbol{M}-\bar{\boldsymbol{M}})^{\mathbf{2}}}\sqrt{\sum(\boldsymbol{O}-\bar{\boldsymbol{O}})^{\mathbf{2}}}}$$

The value of r is such that $-1 < r < +1$. The + and – signs are used for positive linear correlations and negative linear correlations, respectively. If *M* and *O* have a strong positive linear correlation, *r* is close to +1. An *r* value of exactly +1 indicates a perfect positive fit. A correlation greater than 0.8 is generally described as strong, whereas a correlation less than 0.5 is generally described as weak.

3.6 Instability indices

Systematic methods to diagnose the atmosphere's potential to produce severe convective weather can be of great help to forecasters (Tajbakhsh et al., 2012). Instability is a critical factor in the development of severe weather, and severe weather instability indices can be a useful tool when applied correctly to a given convective weather situation. Suresh, (2012) and A J and Mohanty, (2008) had described in details on the different thermodynamic indices. The use of indices may varies from country to country, with different critical values. And there are several indices that signify the instability

parameters used in thunderstorm forecasting. Instability indices use in this study are describes below.

Convective Available Potential Energy (CAPE): CAPE indicates the amount of buoyant energy available as the parcel is accelerated upward. Higher the CAPE value more is the instability and the greater potential for strong and perhaps severe convection.

$$CAPE\left(\frac{J}{Kg}\right) = g\int_{Z_{lfc}}^{Z_{lnb}} \frac{T_{ve} - T_{vp}}{T_{ve}}\, dZ$$

CAPE is measured in unit of Joules/kg. It is the measure of the ratio of difference between the parcel temperature and environment temperature to environment temperature and vertically integrated from the level of free convection to the equilibrium level times acceleration due to gravity.

Table 3.2. Critical value of CAPE

CAPE	**Condition**
Below 0	Stable
0 to 1000	Marginally unstable
1000 to 2500	Moderately unstable
2500 to 3500	Very unstable

(National Weather Service)

Convective Inhibition (CIN): CIN represents the amount of negative buoyant energy available to suppress upward vertical acceleration, or the amount of work the environment must do on the parcel to raise the parcel to its LFC. CIN basically is the opposite of CAPE, and represents the negative energy area on the sounding where the parcel temperature is cooler than that of the environment. The smaller the CIN is, the weaker must be the amount of synoptic and mesoscale forced lift to bring the parcel to its LFC and Higher the CIN is, no lift can suppress convective development, despite possibly high CAPE values, the stronger must be the amount of synoptic forced lift to bring the parcel to its LFC. CIN is usually the result of a capping stable layer or inversion, with values of over 200 J/kg significantly inhibiting convective potential.

$$CINE\left(\frac{J}{Kg}\right) = g\int_{Z_{ground}}^{Z_{top}} \frac{T_{vp} - T_{ve}}{T_{vp}}\, dZ$$

Total Total Index (TT): The Total Total Index is severe weather index calculated as the sum of the vertical total and the cross total. The vertical total represents the lapse rate between 850mb and 500mb whereas the cross total gives 850mb dew point temperature or the moisture at 850mb pressure level. Higher value of temperature and dew point temperature at 850mb and lower temperature at 500mb increases the instability in the atmosphere.

$$TT = T(850mb) + Td(850mb) - 2T(500mb)$$

Where T and Td in degree C represent the temperature and dew point temperature at the given level respectively.

Table 3.3. Critical value of Total Total Index

TT	**Event**
44	Thunderstorms
50	Severe thunderstorm possible
55 or greater	Severe thunderstorms likely, possible tornadoes

(http://tornado.sfsu.edu/geosciences/classes/m201/buoyancy/SkewTMastery/mesoprim/sk

K index: K index is useful for diagnosing the potential for convection which is based on the vertical temperature lapse rate and extent of low level moisture in the atmosphere.

$$KI = T(850mb) - T(500mb) + Td(850mb) - [T(700mb) - Td(700mb)]$$

Table 3.4. Critical value of K index

K Index	**Event**
Below 30	Severe weather possible
Over 30	Better possible for thunderstorm with heavy rain
K= 40	Best possible for thunderstorm with heavy rain

(National Weather Service)

Since K index include the dew point depression at 700mb, dry air present in this layer will lower the value. In general, higher the ambient k index value the greater the potential for heavy rain.

Precipitable water: Precipitable water is the amount of water potentially available in the atmosphere for precipitation, usually measured in a vertical column that extends from the Earth's surface to the upper edge of the troposphere. The total atmospheric water vapour contained in a vertical column of unit cross-sectional area extending between any two specified levels, commonly expressed in terms of the high to which that water substance would stand if completely condense and collected in a vessel of the same unit cross section. If x(p) is the mixing ratio at the pressure level p, then the precipitable water vapour (W) contained in a layer bounded by pressure P1 and P2 is given by

$$W = \frac{1}{\rho g} \int_{P1}^{P2} x dP$$

Where ρ is density of water and g it the gravity.

3.7 Flowchart

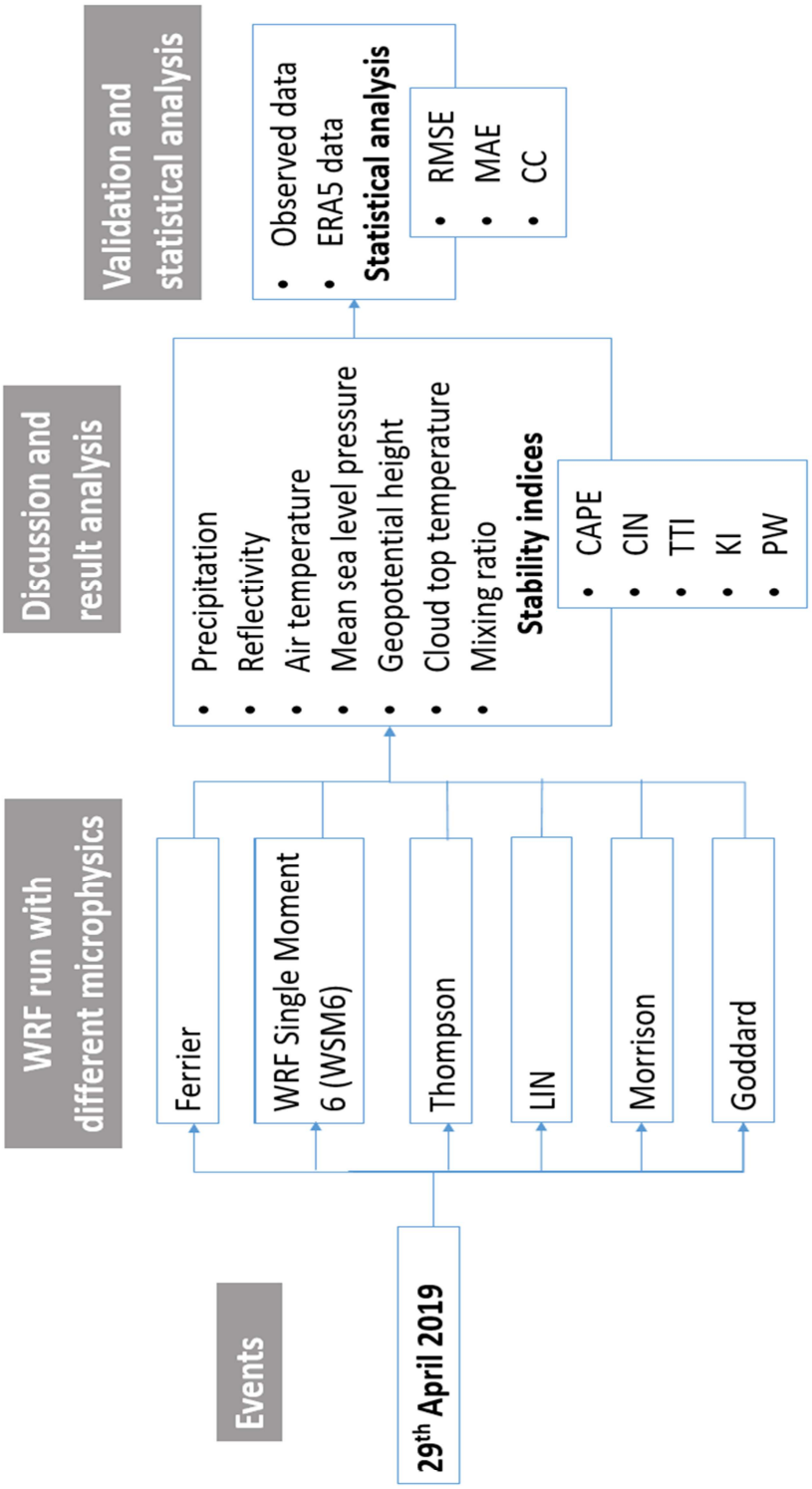

Figure 3.4. Flowchart of methodology

CHAPTER 4

4 RESULTS AND DISCUSSION

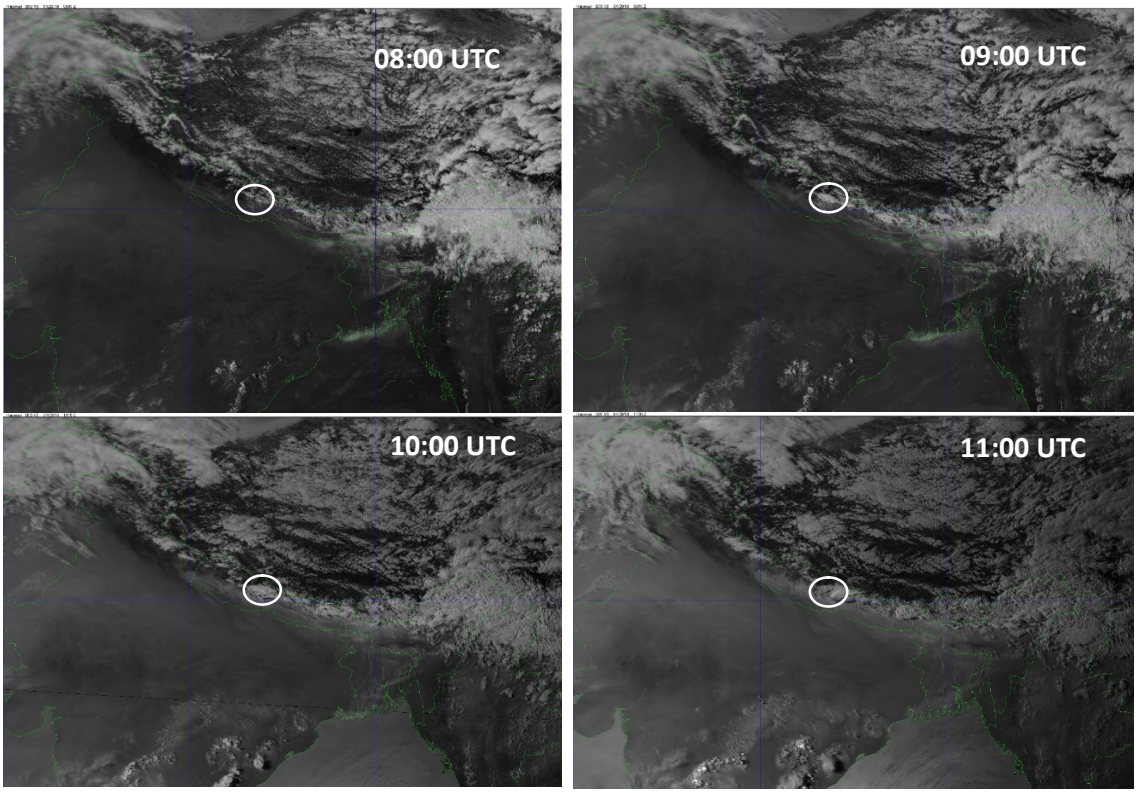

Figure 4.1Himawari-Satellite infrared imageries 29th April 2019 at (0800, 0900, 1000 and 1100 UTC). The white circle indicate the Pokhara region

4.1 Satellite View

The Pokhara valley is surrounded in the east, north and northwest by high mountains which act as barriers and induce precipitation from orographically lifted humid air. Precipitation results also from mountain-valley flows that are drawn into the area each day. These features explain why Pokhara is a moisture convergence zone that receives some of the highest precipitation in Nepal. On 29th April 2019, Golf-ball-sized monster hail inflicted heavy damage to crops in Pokhara, Nepal within 30 minutes. Himawari-8 satellite infrared imageries are shown in Figure 4.1 provide the insight of storm formation and it dissipates. White circle in the image indicate the Pokhara region. In the images, the North Indian plains and south Nepal are dark in colour, indicating a warm surface and mostly clear skies. There are some clouds scattered across North of Nepal which indicates presence of humid air and convective activities. The presence of humid air and

convective activity is appropriate for this pre-monsoon period that cause the thunderstorm (Aryal, 2018). The cloud base is increasing with increasing inflow of the moisture. The source of the moisture are from the nearby source. The peak formation of cloud is at 1000UTC and then it starts to dissipate after 1100UTC as seen in Figure 4.1.

4.2 Model Simulation of the event

Synoptic data of Pokhara airport synoptic station of 29th April 2019 provided by DHM shows that the total precipitation of the day is 41mm whereas the precipitation of 3hr (0900UTC to 1200UTC) was 40.5mm. The temperature recorded at 0900UTC was 30.8 which was drop to 19.2 degree Celsius by 1200UCT. As the synoptic data recorded every 3 hr detailed information on the event was not possible. One day precipitation plotted form the IMERGE data (Figure 4.2) shows the spatial variation. It had captured the image but spatially shifted to east. Below are model outputs with different parameter regarding the event.

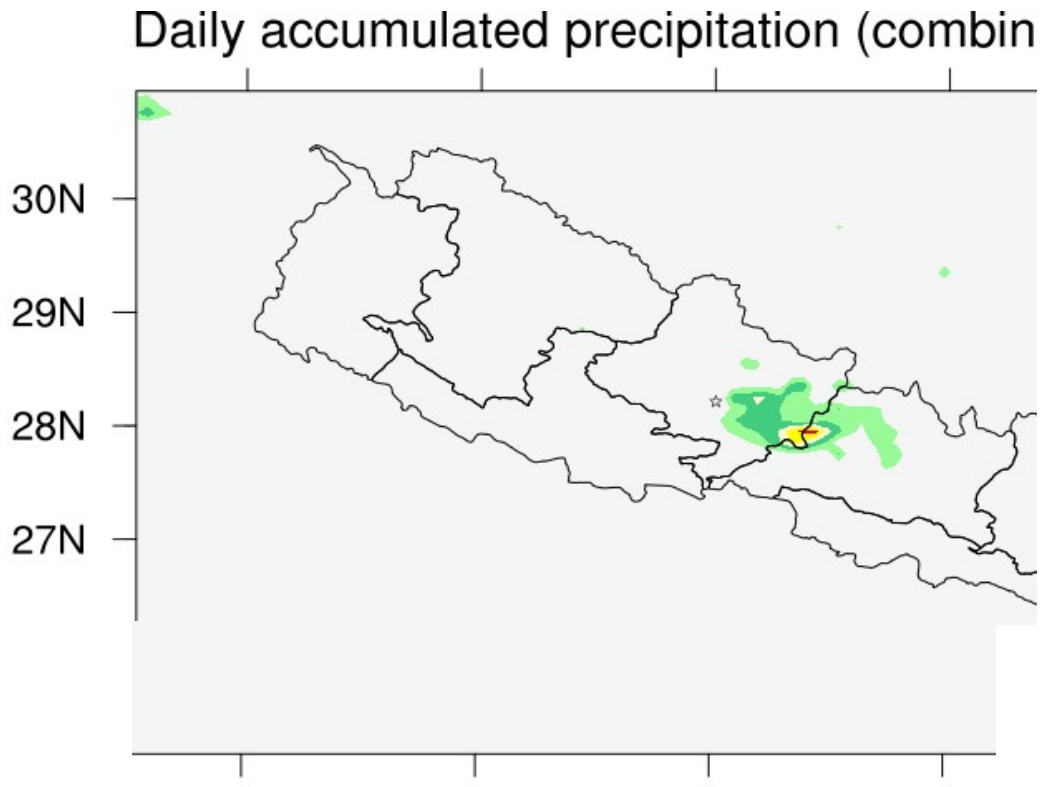

Figure 4.2. One day GPM IMERG precipitation of 29th April 2019

4.2.1 Analysis of Precipitation

One day accumulated rainfall on 29th April 2019 simulated by WRF model runs by various microphysics schemes are shown in Figure 4.3. In all the scheme location of most extreme precipitation is spatially moved towards northeast but has less error as compared

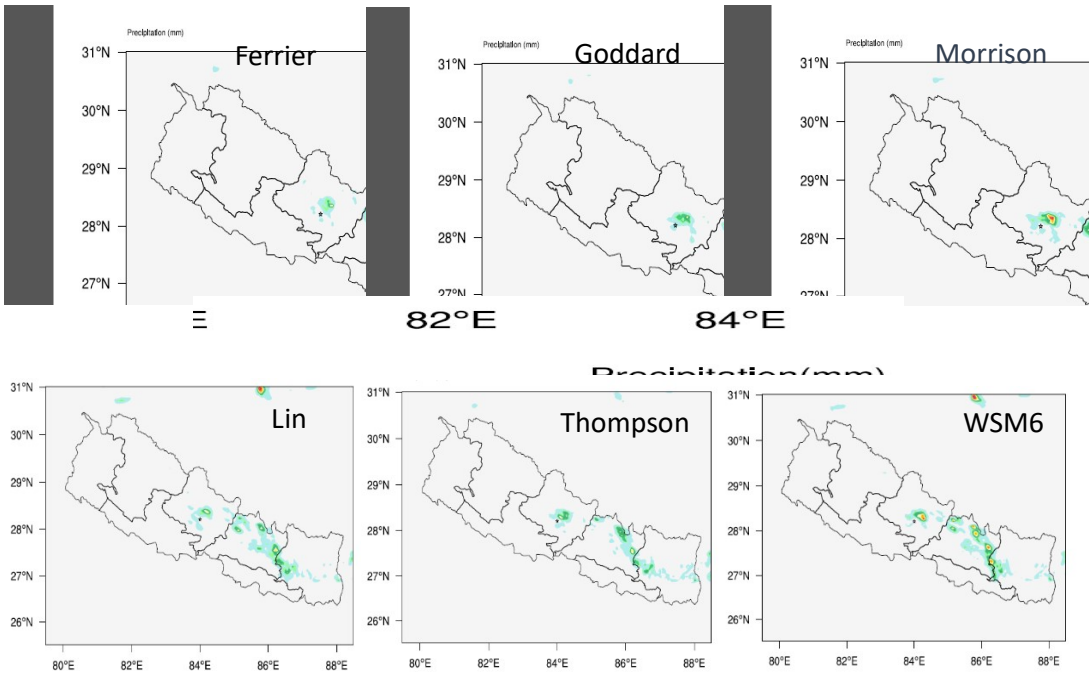

Figure 4.3. One day WRF model precipitation with different microphysics of 29th April 2019

to the IMERGE data in Figure 4.2. All the scheme show precipitation above 30mm to which we can say these scheme are capable to capture the event. The highest rainfall is shown by Morrison microphysics about 48mm whereas the least is shown by Ferrier microphysics. Precipitation amount of Morrison, WSM6 and Thompson are near to the DHM observed one day precipitation. As compared to IMERGE data WRF model has well simulated the event with all the microphysics for the event with small spatial variation.

4.2.2 Analysis of Hydrometeors

Vertical profile of maximum mixing ratio of four different hydrometeor particle species for each microphysics scheme is presented in figure 4.4. It was simulated on average area (28°N, 28.5°N, 83.8°E, 84.2°E) and at specified time 1000UTC. Here, Ferrier scheme produce graupel hydrometeor separately. It produce the graupel hydrometeor species

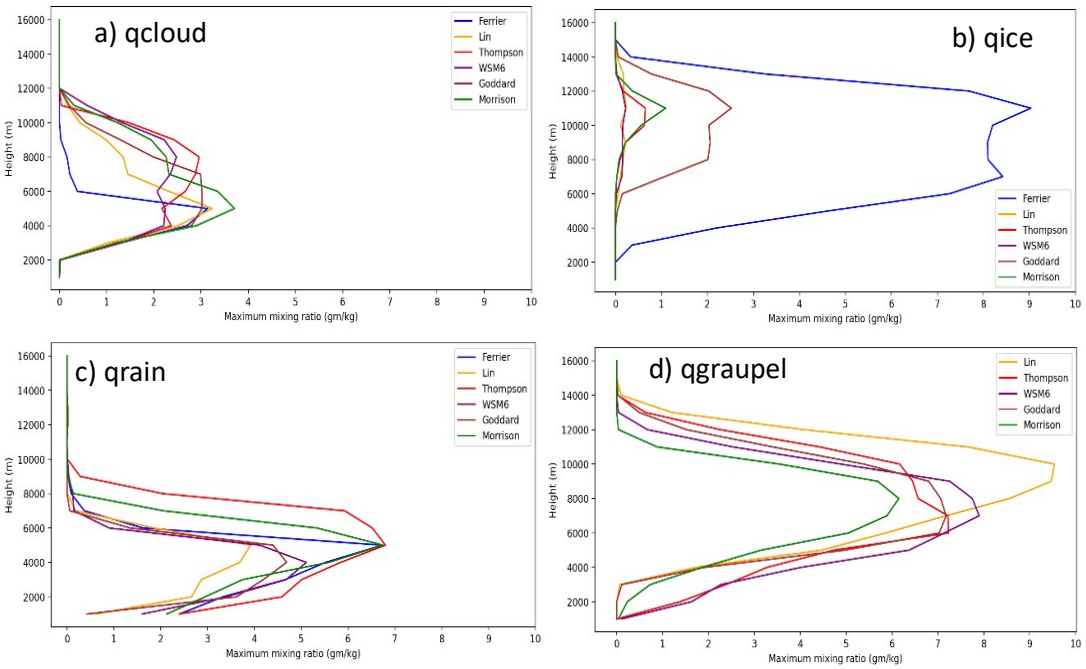

Figure 4.4. Vertical profile of maximum mixing ratio (gm/kg) of hydrometeors on average area for different microphysics schemes.

under ice species. Thus, diagnostic of cloud water, rain and ice species are simulated for Ferrier scheme. So, there is high value in ice species of Ferrier scheme in Figure 4.4(b). Ice hydrometeor show the least number among all other species which is concentrated at 2km above melting layer. The melting layer is the altitude interval throughout which ice-phage precipitation melts as it descends. This presence of ice layer confirms that the cloud storm is typically of convective mix cloud that penetrate up to 14km height. Figure 4.4(a) shows the cloud particles which are more concentrated in the middle layer of cloud storm with base cloud 2km above the surface. It is evident that the Lin scheme produce more graupel (9gm/kg) than other scheme (Figure 4.4(d)). The peak of graupel mass mixing ratio for WSM6, Morrison, Thompson and Goddard are 8, 6, 7 and 7gm/kg respectively. Most of the graupel species are found slightly above the peak melting layer. Thompson and WSM6 scheme produce graupel below the level of the base cloud which indicates that hail may reach the ground since they remain to appear after passing through the melting layer.This confirms that WRF model is able to simulate storm cloud with reasonable vertical condition atmosphere when the hail event occurred.

4.2.3 Analysis of Reflectivity and Cloud Top Temperature

The spatial pattern of maximum reflectivity (dbz) has been presented for different microphysics scheme during the time of event occurred (Figure 4.5). All the scheme produce more than one core cloud echo during the time with the maximum reflectivity in cloud core above 40dbz. But at the station point, none of the scheme can capture high maximum reflectivity. Identifying the better scheme for the reflectivity is difficult as there is not any reflectivity data for comparison.

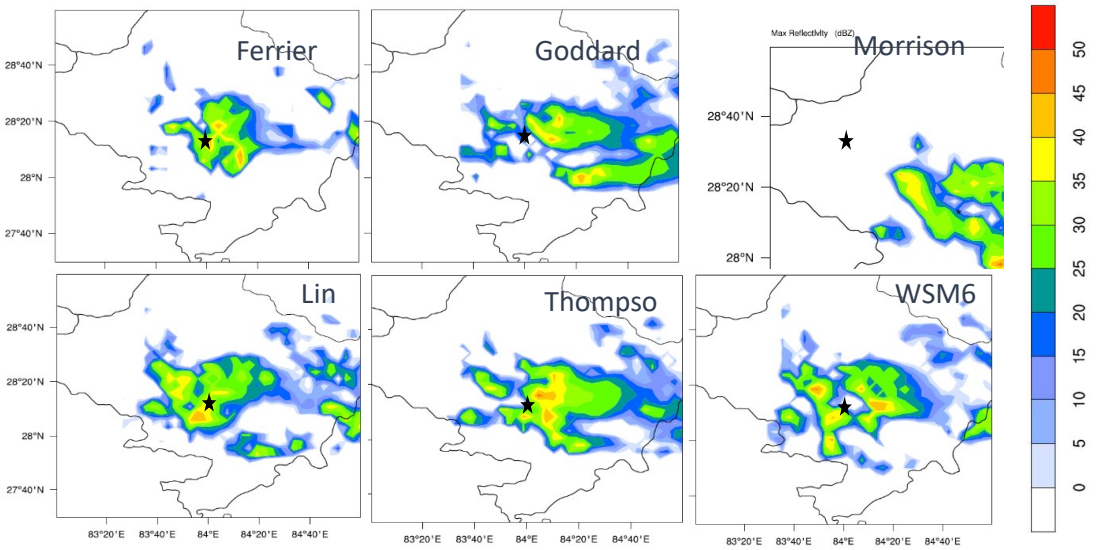

Figure 4.5. Reflectivity (dbz) for different microphysics at 10UTC.

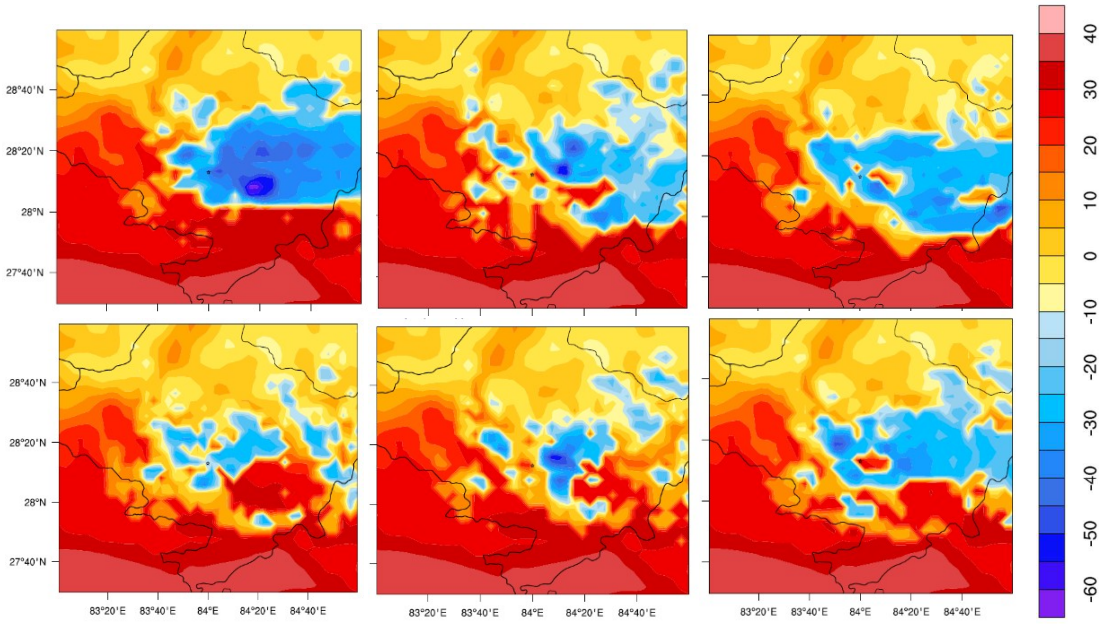

Figure 4.6. Cloud Top Temperature (°C)for different microphysics at 10UTC.

Similarly, the ability to accurately forecast cloudiness is necessary in the field of aviation. Brightness temperature and cloud top temperature derived from NWP model output have been used to demonstrate the advanced capabilities of these models for severe weather prediction (Otkin and Greenwald 2008). Figure4.6 shows the spatial pattern of Cloud Top Temperature (CTT) for different microphysics during event time. All the scheme shows CTT below -30°C where Ferrier, Thompson and Goddard shows below -50°C. There areno data available for validation but it is good enough CTT for thunderstorm to occur.

4.2.4 Instability Indicator

Variation of convection in the atmosphere depends upon dynamic as well as thermodynamic instability indices. A number of stability indices have been devised in order to detect the likely occurrence of thunderstorms. To examine different stability indices namely Convective Available Potential Energy (CAPE), Total Total Index (TTI), K Index (KI) and Precipitable water obtained from operational WRF-ARW model for thunderstorm studies over Pokhara. The model results are not able to compare with observed stability indices due to unavailability of observed data. Table 4.1 shows the ARW model simulated stability indices with six microphysics scheme (WSM6, Ferrier, Thompson, Lin, Goddard and Morrison) over Pokhara on 29th April 2019. Values are obtained before 6 hours 3 hours and around event time at 0400UTC, 0700UTC and 1000UTC, respectively.

The CAPE represents the amount of buoyant energy available to accelerate a parcel vertically and a CAPE value greater than 1500 Jkg−1 is necessary for supercells to form (Johns and Doswell, 1992).Similarly, large values of CIN is an indication of stable atmosphere and such atmospheric situation is not favorable for thunderstorm event even though the other factors are favourable for the occurrence of convective activities (Ahasan M.N., S. K. Debsarma, 2015). The low value of CIN along with the high value of CAPE is clear indication for the formation of thunderstorm events (Paul et al., n.d. , 2019).The model simulated CAPE values for all microphysics are high and greater than the critical level from 6 hours before the thunderstorm with CIN value much lesser than its critical value (0.1).after the event, the CAPE value decrease rapidly with increase of CIN may be because of the cooling of the earth surface by precipitation.

The KI is a combination of the Vertical Totals (VT) and lower tropospheric moisture characteristics. The VT is the temperature difference between 850 and 500 hPa, while the moisture parameters are 850 hPa dewpoint and 700 hPa dewpoint depressions.

Table 4.1 The thermodynamic indices over Pokhara station during 0400UTC, 0700UTC and 1000UTC for different microphysics.

Microphysics	Time	CAPE (j/kg)	CIN (j/kg)	TT Index (°C)	K index (°C)	Perceptible water (mm)
Thompson	04:00 UTC	**1701.04**	**0.10**	**52.15**	28.44	26.95
	07:00 UTC	**1505.30**	**0.10**	**53.53**	**41.53**	31.12
	10:00 UTC	1166.67	115.4	**51.91**	**41.90**	**35.51**
Ferrier	04:00 UTC	**1830.78**	**0.10**	**52.32**	28.72	27.19
	07:00 UTC	**1561.53**	**0.10**	**53.6**	**40.7**	31.15
	10:00 UTC	618.70	163.7	**50.33**	**44.17**	**37.24**
LIN	04:00 UTC	**1787.83**	**0.10**	**52.09**	28.54	27.58
	07:00 UTC	**1584.57**	**0.10**	**53.59**	**42.68**	31.76
	10:00 UTC	572	9.97	43.77	**38.22**	**42.96**
WSM6	04:00 UTC	**1802.31**	**0.10**	**52.35**	28.34	27.08
	07:00 UTC	**1588.8**	**0.10**	**53.58**	**40.51**	31.57
	10:00 UTC	428.98	155.9	**50.36**	**43.36**	**36.37**
Goddard	04:00 UTC	**1673.96**	**0.10**	**52.18**	27.62	26.57
	07:00 UTC	**1538.05**	**0.10**	**53.66**	**40.01**	31.03
	10:00 UTC	1330.51	62.34	**53.52**	**46.13**	**36.39**
Morrison	04:00 UTC	**1756.49**	**0.10**	**52.208**	28.59	27.13
	07:00 UTC	**1544.88**	**0.10**	**53.63**	**41.31**	31.47
	10:00 UTC	275.88	234.06	**53.74**	**42.11**	**35.23**

The KI has proved useful in indicating the probability of severe thunderstorms. As the KI increases, so does the probability of having a severe thunderstorm (Source: AWS Technical Report 1990). Table 4.2 shows the KI values for all microphysics greater than the critical value before 3 hours and at the time of thunderstorm as well which is favourable for thunderstorm occurrence.

Miller (1972) introduced the TTI for identifying areas of potential thunderstorm development. It accounts for both static stability and the presence of 850 hpa moisture. A TTI of greater than 44 indicates favourable conditions for the development of severe thunderstorms (Source: AWS Technical Report 1990). The model simulation with all microphysics shows the TTI value greater than the critical value before 6 hours and at the time of thunderstorm indicating severe weather phenomenon in the region.

The precipitable water indicates the total humidity of the air above a location, and is a good indicator of the amount of moisture potentially available to supply rainfall. Higher values mean that more water is available for potential rainfall. Precipitable water values of greater than 31.8 millimetres (1.25 in) favour the development of organized thunderstorm complexes (Maddox et al., 1979). In the model simulation with different microphysics, all schemes shows the perceptible water values above critical values.

To sum up, WRF-ARW model with different microphysics simulated stability indices for the thunderstorm over Pokhara on 29th April 2019 clearly indicated that ARW model has well captured the instability of the atmosphere for the occurrence of a severe thunderstorm over Pokhara.

4.3 Comparison with Observation

The model outputs are compared with the observed data provided by DHM. Air temperature and sea level pressure are taken from the Pokhara airport synoptic station. 12 hours data at interval of hour form 0000UTC to 1200UTC is compared with model point data of same time period and same latitude and longitude of Pokhara station. Rainfall data are taken from AWS Lumle station which is around 24km away from Pokhara sataion. Further statistical analysis tool RMSE, MAE and Correlation coefficient are used.

4.3.1 Precipitation

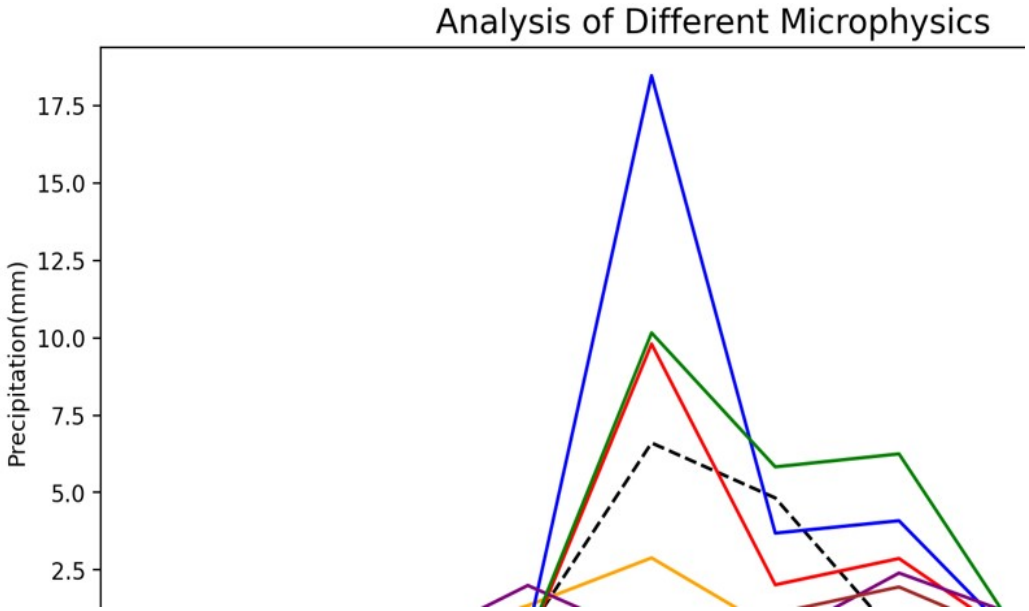

Figure 4.7. Time series of half hourly precipitation of model output for different microphysics and AWS datafrom 0800UTC to 1230UTC.

Half hourly rainfall model output and AWS are shown in Figure.4.7. Red line represents the AWS station data which shows the peak rainfall at 1000UTC. The rainfall produced by the WRF runs with microphysics schemes from single moment (Lin, WSM6 and Goddard) which only simulate the accumulated mass concentration of each hydrometeor species does not shows good correlation and underestimate the rainfall as compared to AWS data. While the rainfall produced by the WRF runs with microphysics scheme form double moment (Thompson, Ferrier and Morrison) which consider both the mass and the number concentration of hydrometeors shows good correlation but overestimate the rainfall as compare to AWS data. Thompson scheme has the peak rainfall of 9.8mm which is nearest to AWS peak rainfall 6.604mm. From the calculated error statistics Table 4.2, it is seen that the Thompson scheme produce minimum RMSE(1.65) followed by Lin(1.85) and then by Morrison(2.27). While the Lin scheme produce minimum MAE(1.1) followed by Thompson(1.17) and then by Morrison(1.34). In case of Correlation coefficient, Ferrier shows the high correlation (0.85) followed by Thompson (0.83) and then by Morrison (0.82).It is found that, though a collective implication on all errors cannot be obtained in one scheme, on average Thompson and Morrison scheme could produce the least MAE and RMSE along with maximum correlation coefficient.

4.3.2 Sea Level Pressure

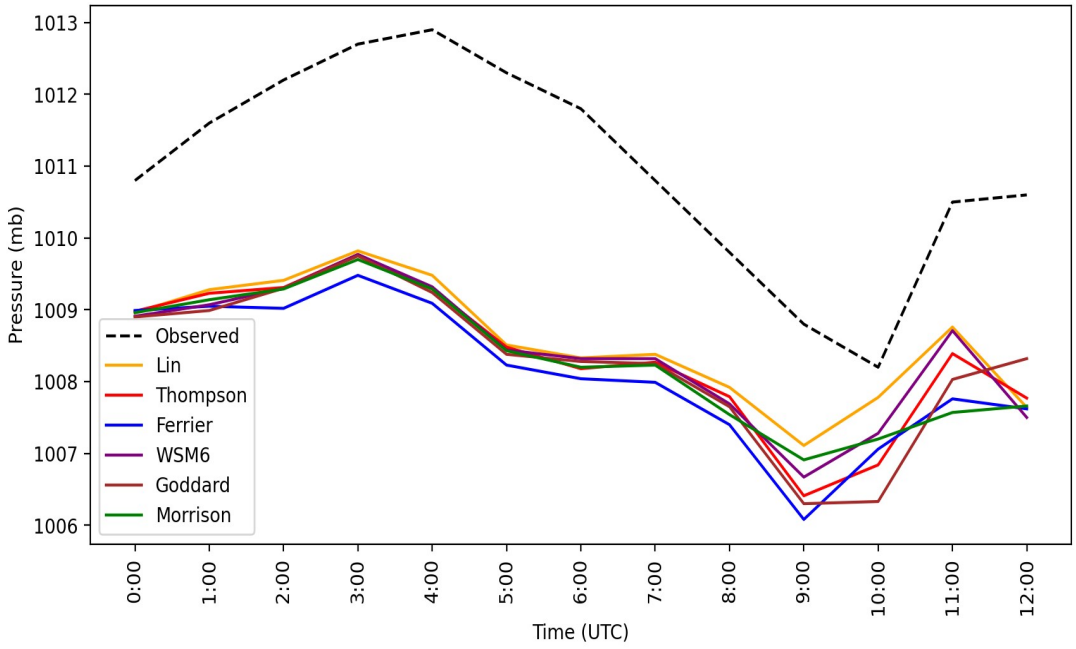

Figure 4.8. Time series of hourly Sea Level Pressure of model output for different microphysics and observed data from 0000UTC to 1200UTC.

Sea level pressure model output of different microphysics and observed data form 0000UTC to 1200UTC are shown in Figure 4.8. WRF output form all the microphysics underestimate the SLP and it captures earlier of the SLP falling before it agrees with observation. Although for each scheme the magnitude is slightly different about 2mb, the pattern of increasing and decreasing of SLP is similar to the observed data. When the warm air is forced up due to strong convection, it will trigger the surface air pressure drop. And when the precipitation starts, the convection processes stop and gradually the surface air pressure increase. Table 4.2 shows Lin perform the minimum RMSE(2.59) and then WSM6 (2.71), Thompson (2.73), Goddard (2.79), Morrison(2.79) and Ferrier(2.96), respectively. Similarly, Lin scheme also produce minimum MAE (2.43) and then WSM6(2.59), Thompson (2.64), Morrison (2.68), Goddard (2.79) respectively. On analysing Correlation coefficient Goddard scheme shows the high correlation (0.91) and then by Thompson (0.88). Here also a collective implication on all errors is not obtained in one scheme but all the schemes show good correlation and less errors.

4.3.3 Air Temperature

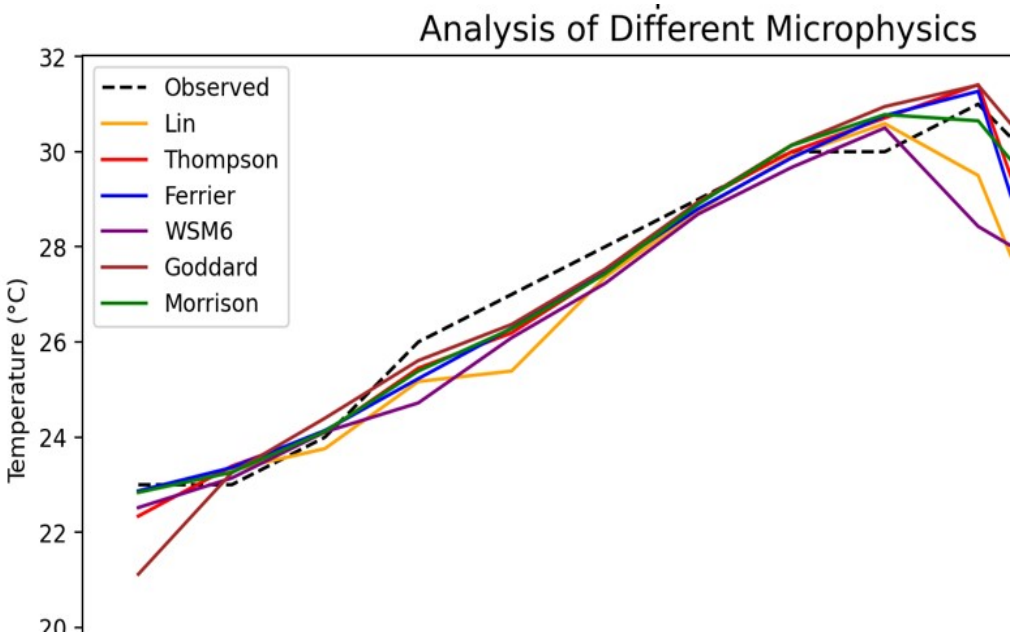

Figure 4.9. Time series of hourly Temperature (°C) of model output for different microphysics and observed data from 0000UTC to 1200UTC.

Air temperature model output of different microphysics and observed data form 0000UTC to 1200UTC are shown in Figure4.9. At earlier the temperature gradually increase till 0900UTC and then start to decrease as increase in Cumulonimbus (Cb) cloud and rapid decrease after the event. WRF output form all the microphysics well simulate the air temperature as it shows similar pattern too but the decrease of temperature after the event is less compared to observed (19°C). Observing the error statistics table 4.2, for air temperature all scheme shows almost similar values as they follow similar pattern. But if we go deeply Goddard scheme shows the minimum RMSE(2.19) and also produce minimum MAE (1.23). Similarly, in Correlation coefficient Goddard scheme shows the high correlation (0.84) and then by Lin (0.78).

Overall we could find different microphysics scheme are good for different parameters. But on averaging the error of air temperature, SLP and precipitation for respective microphysics scheme, we could find that Thompson and Morrison has high correlation with observed data.

Table 4.2. Statistical error analysis of precipitation, SLP and Air temperature for different microphysics.

Microphysics		Ferrer	Goddard	Morrison	Lin	Thompson	WSM6
AWS Precipitation	**RMSE**	3.99	2.41	2.27	1.85	1.65	2.64
	MAE	1.97	1.46	1.34	1.09	1.17	1.64
	CC	0.85	0.20	0.82	0.74	0.83	-0.18
Sea Level Pressure	**RMSE**	2.96	2.79	2.79	2.59	2.73	2.71
	MAE	2.86	2.71	2.68	2.43	2.64	2.59
	CC	0.85	0.91	0.87	0.81	0.88	0.85
Air Temperature	**RMSE**	2.95	2.19	2.87	2.39	2.91	2.69
	MAE	1.67	1.23	1.46	1.55	1.63	1.65
	CC	0.66	0.84	0.70	0.78	0.67	0.72
Mean	**CC**	0.78	0.65	**0.80**	0.78	**0.80**	0.46

4.4 Analysis of Atmospheric Process

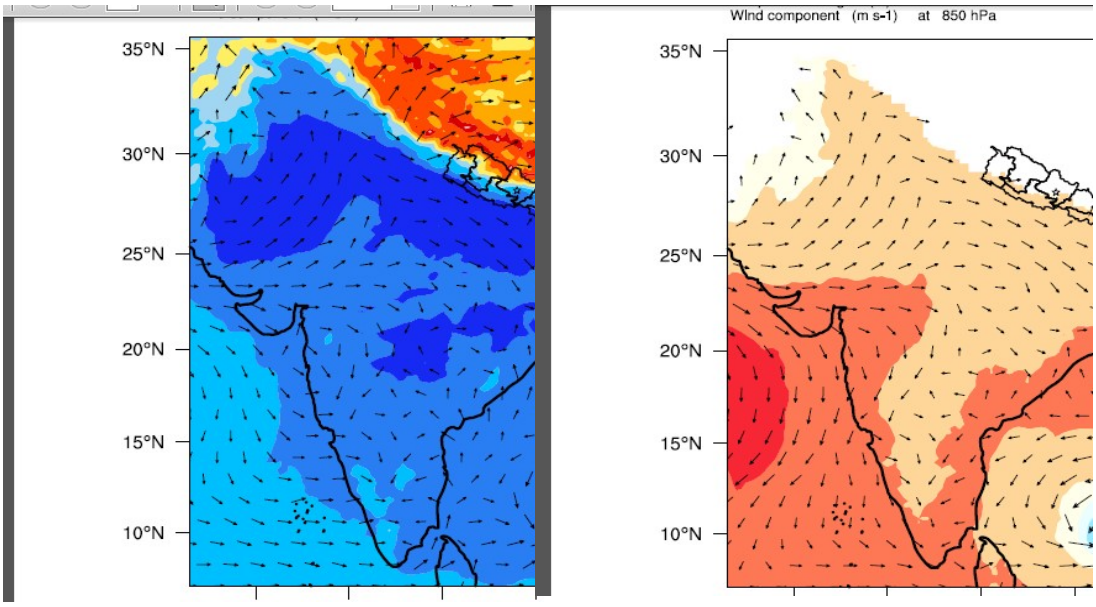

Figure 4.10. Model simulated MSLP with surface wind(left) and geopotential height with wind vector at 850mb (right) at 0900UTC.

The atmospheric process during the event on 29th April is analysed using model data as well as ERA5 data. As from previous section, Thompson and Morrison scheme simulate well with high correlation with observed data, Thompson scheme is used for further study of atmospheric process of the event with domain 25km grid spacing for synoptic features.

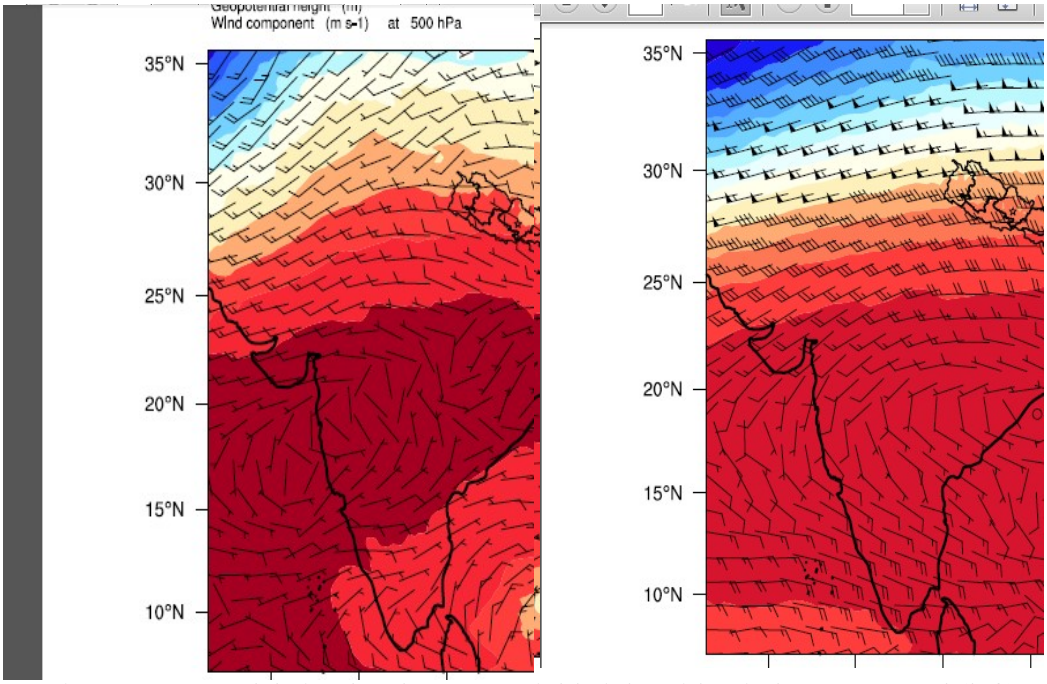

Figure 4.11. Model simulated geopotential height with wind vector 500mb(left) and 300mb (right) at 0900UTC.

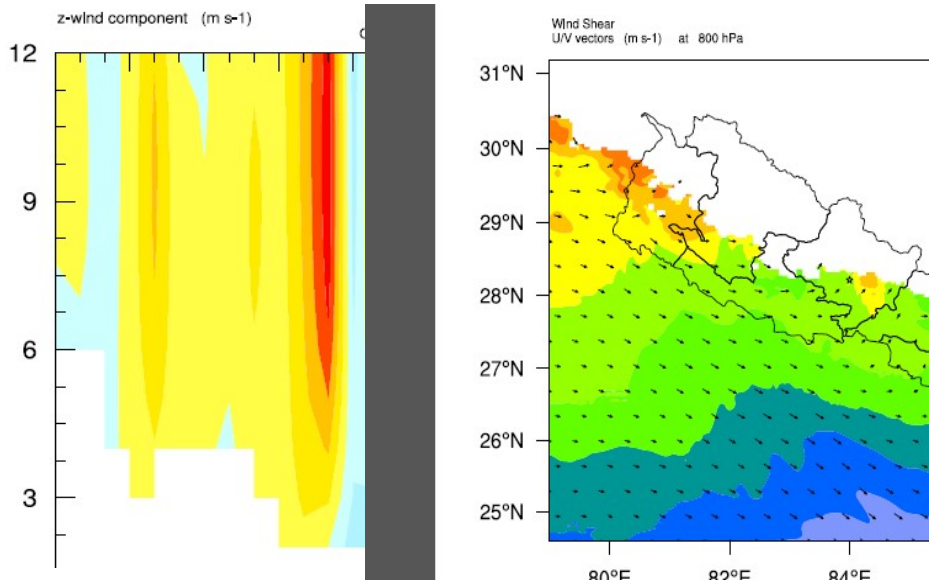

Figure 4.12. Vertical Velocity(m/s) on longitude line between 83.5 to 84.5E (left) and wind shear between 800mb and 200mb (right)1000UTC.

Figure.4.10 depicts MSLP with surface wind vector and geopotential height with wind vector at 850 hpa form model data. Low pressure system was seen from the beginning of the day at south Terai plain of Nepal, north India and Northwest India. Low pressure belt goes on intensifies with time. With increase in heating form the sub-tropical sun provide a suitable condition for convective Activity. Cold continuous movement of mid-tropospheric waves "Western Disturbances" across the foothill of Himalaya is found with very active sub-tropical jet stream from the 500hpa and 300hpa wind and geopotential height (Figure 4.11). The presence of subtropical jet stream at upper level provides a mechanism for strong vertical wind shear, thus favouring development of severe convection (Ahasan et al., 2015). The cross sectional (E-W) profile of vertical velocity shows the strong convection at the event area (Figure 4.12). The strong vertical velocity coincides with the region of high relative humidity confirms the development of strong moist convection which is confirmed by the Figure 4.13. And Wind shear between 800 and 200hpa shows above 40m/s at event area during the time of event (Figure 4.12) as the severity of convective storms is influenced by the vertical extend of wind shear (Singh et al., 2017). These presence of strong vertical wind shear, strong vertical velocity with high relative humidity at the region has resulted the intense convective activity in the region and may be a triggering factor.

To compare the Model synoptic data, the ERA5 reanalysis dataset was used. MSLP with surface wind and geopotential with wind vector at 850mb, 500mb and 300mb were plotted (Figure 4.15 and 4.16). Both mode and ERA5 shows similar pattern. In MSLP plot from ERA5 data area of low pressure was concentrated to North of India and south Terai of Nepal whereas it was even larger in model output which includes northwest India. Both show the very strong jet stream at upper level and strong winds shear.

Advection of moisture and their lifting is necessary for the convective activity. Low pressure area signifies the zone of convergence of air mass. It provides suitable condition for moisture flow from the nearby areas. Figure4.13 shows the water vapor mixing ratio (800mb) and vertical profile of relative humidity. The presence of water vapor mixing ratio above 14gm/kg around event area and relative humidity extended upto 250mb vertically clarify the high convective activity. The vertical velocity of above 2m/s at event area is simulated by the model also indicates strong updraft over the event area.

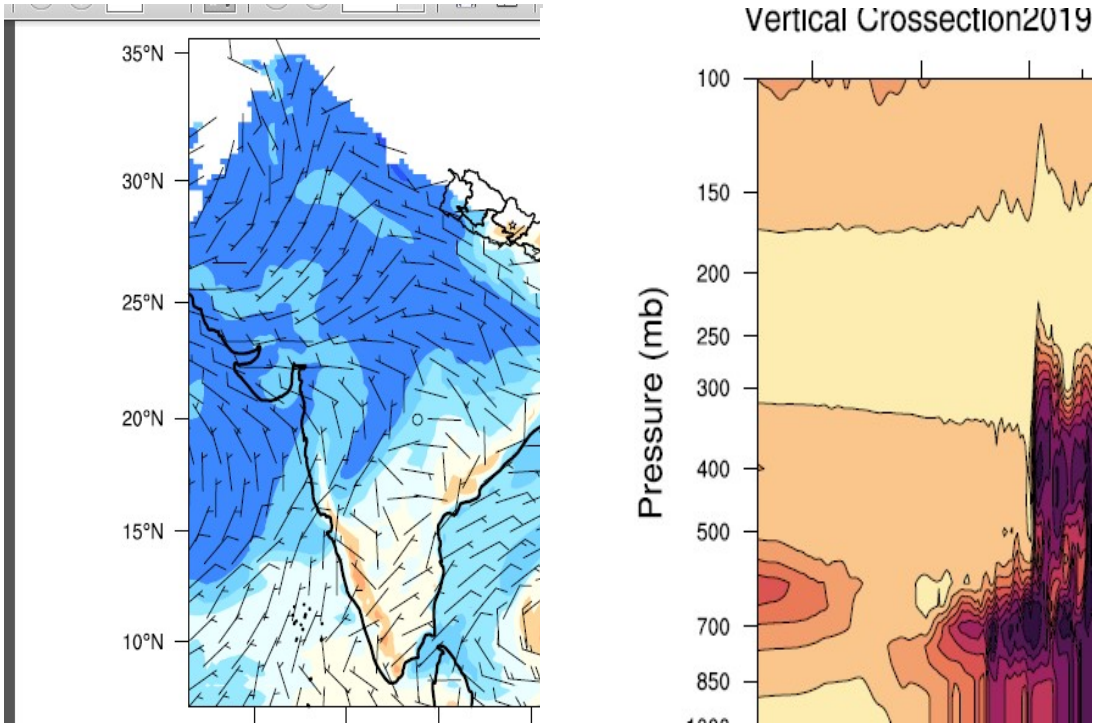

Figure 4.13. ERA5 plot MSLP with surface wind(left) and geopotential height with wind vector 850mb (right) at 0900UTC.

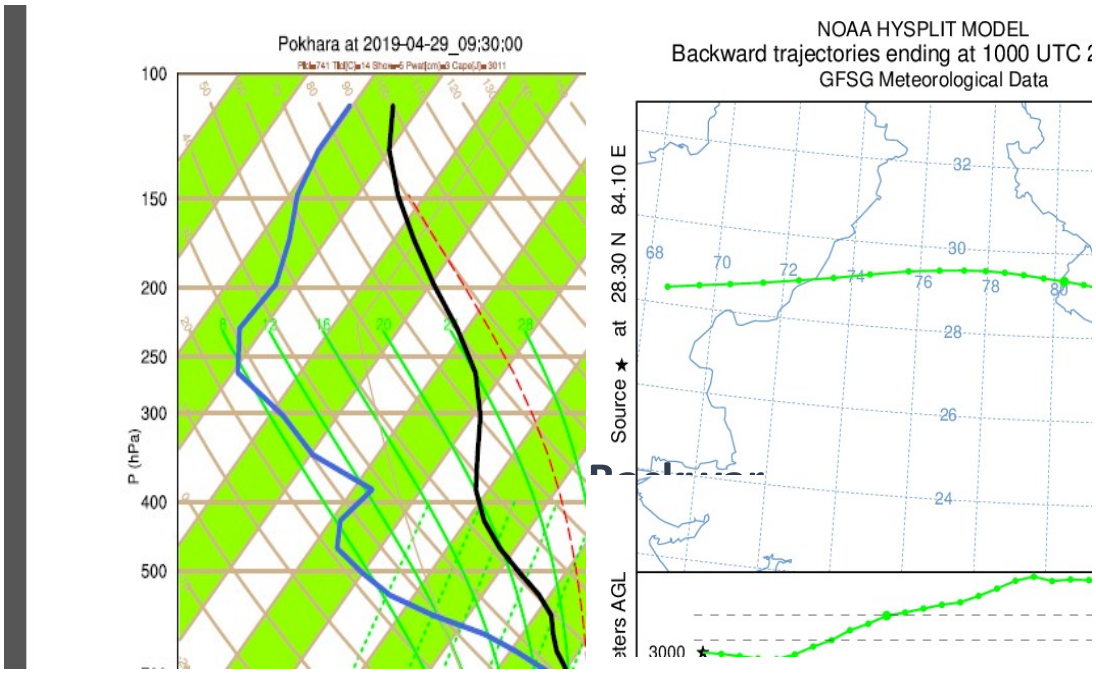

Figure 4.14. Skew-T diagram of vertical atmosphere from model (left) and Backward trajectories plot (right) at Pokhara (28.217E,84.0N) at 1000UTC.

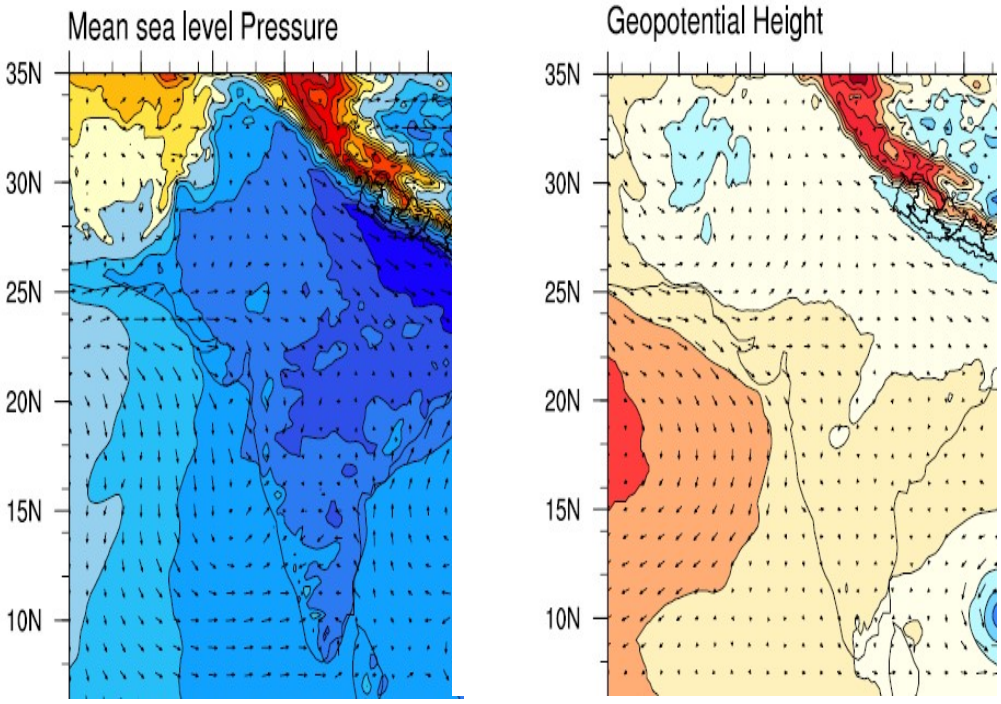

Figure 4.15. ERA5 plot MSLP with surface wind(left) and geopotential height with wind vector 850mb (right) at 0900UTC.

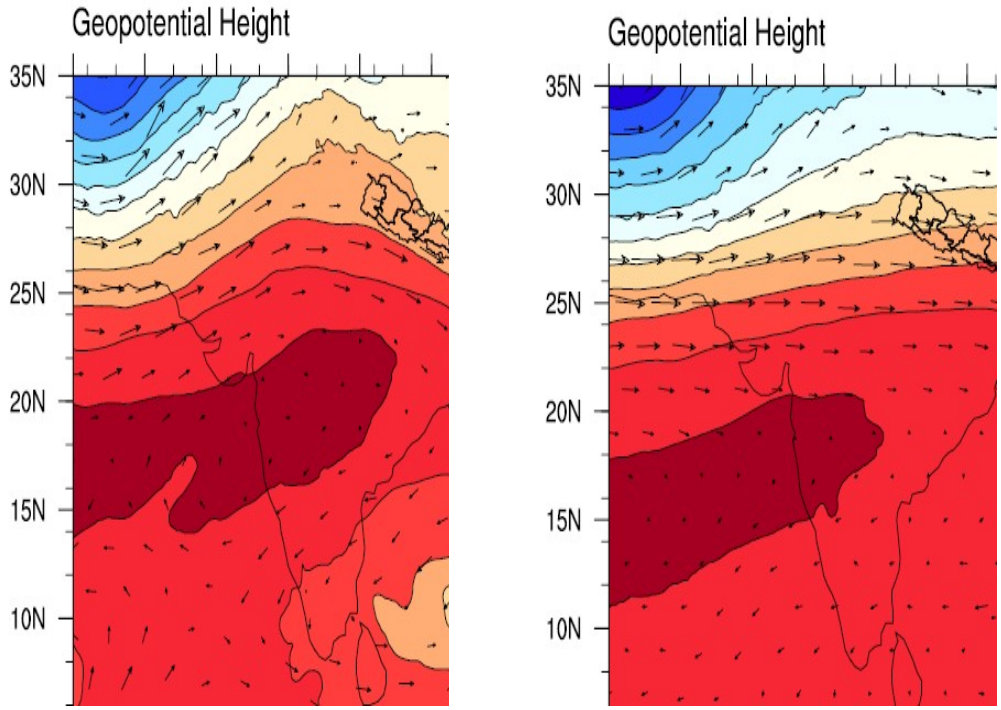

Figure 4.16. ERA5 simulated geopotential height with wind vector 500mb(left) and 300mb (right) at 0900UTC.

For the study of atmospheric condition skew-T plot is generated from the model output at Pokhara station for 1000UTC (Figure.4.14). A Strong vertical wind shear is present in the plot because of wind direction and wind gradient. The direction of surface wind doesn't very much, it is westerlies and may be because of strong impact of Jet stream. The highest CAPE values given by sounding is 3011 J/kg . Convective activity were more favourable during this time period of a day. CAPE is seen to be decreasing afterwards due to the cooling of land mass from precipitation and decrease in the surface temperature.

Further, NOAA HYPSLIT back-trajectory model was run for 1000 UTC 29th April 2019 back to 24 hours a at Pokhara station to identify the moisture source (Figure 4.14). It is simulated at three different level (500, 1500 and 3000 meter AGL(Above Ground Level). The red, blue, green lines in figure represent the height of 500, 1500 and 3000m AGL respectively. The model output shows that the moisture in the lower level below 1 km is converged from the nearby areas in east. The middle level around 1500m moisture source is converged form the west direction within Nepal. And at the upper level around 3000km or above moisture was carried from the far region Pakistan. The intrusion of hot dry airmass from the south and the moist airmass from the north act as the favourable condition for the initiation of convection in the region.

CHAPTER 5

5 DISCUSSION

Study of thunderstorm could be evaluated through different parameters for the simulation of the thunderstorm properties as well as for the prediction. In this research, simulation of research is done by stability indices, reflectivity, and cloud top temperature with six different microphysics schemes implemented in the WRF-ARW model. All the microphysics shows the values of stability indices above the critical value. Average value of the CAPE was above 1700J/kg with minimum CIN and TTI and KI value greater that the threshold value before 6hr of the event. The precipitable water meet the threshold value at 1000UCT. This could be more relevant in this event as the event was hail storm. Ceperuelo (2006) found the low precipitable water content in the thunderstorms helps to develop hailstorms as the weight of moisture and water will reduce the strength of the updrafts. Similarly the presence of multiple core cloud with negative cloud top temperature and high reflectivity supports for the development of severe thunderstorms.

Model simulated synopsis of atmospheric conditions shows a favourable atmosphere for the convection. Presence of low pressure system at the south of Nepal which goes on intensifying with time and cold continuous movement of mid tropospheric wave "western disturbances" across the foothills of the Himalaya is found. A quote from Bob Banta, "In complex, elevated terrain, all necessary conditions for thunderstorm initation are almost always present." is applicable to the Himalayan foothills of Nepal during the pre-monsoon month April (Aryal et. al., 2018). All the basic requirement for the thunderstorm, high relative humidity, strong vertical updraft, wind share are found from the model result. The triggering point of the hail storm could be the high speed subtropical jet shifting from north to south directly overhead of the Pokhara region creating strong wind share.

In use of different microphysics, through comparison and statistical analysis Thompson and Morrison microphysics performed well than other microphysics. Similar result was obtained in the study of extreme precipitation event over the Centeral Himalaya (Karki et. al, 2018). Previous studies found that the Thompson microphysics scheme as most suitable one on comparison with six different microphysics (CAM, WDM6, NSSL2, Milbrandt, Morrison and Thompson). The result was also supported by (Rajeevan et al.,

2010; A. J. Litta et al.,2013; R. Mohan et al., 2018; Sari et al., 2018) that found Thompson scheme more reliable under simulation with different microphysics.

CHAPTER 6

6 CONCLUSION AND RECOMENDATION

A severe thunderstorm event on 29th April 2019 over the Pokhara is simulated in the study. The sensitivity of six different microphysics scheme using WRF-ARW model has been discussed. Examine the exact time and location of the thunderstorm require more study with high resolution data and minimum time step. Taken into account the use of different microphysics schemes are not sensitive enough as different scheme are good at different parameters. Thus considering the best microphysics which can simulate thunderstorm with hail appropriately remains difficult. However comparing with observed and using statistical error analysis Thompson and Morrison are relatively better scheme for the simulation of thunderstorm.

The conclusions of the study are as follows:

- WRF-ARW model is able to simulate the thunderstorm event on 29th April over the region with small spatial-temporal variation.
- All the microphysics used in sensitivity experiment well simulated the event with better result by the inner domain of 1km.
- On the examination of model simulated stability index, all have has well captured the instability of the atmosphere for the occurrence of a severe thunderstorm.
- Overall Morrison and Thompson scheme performed well with same correlation coefficient of 0.80, whereas WSM6 has least results with mean correlation coefficient of 0.46 compared to the observed.

WRF model can be the useful tool for forecasting and studying the extreme events. The model has simulation well over the Pokhara region. Based on above study, Thompson and Morrison are comparatively well perform over the study region. But requires more study to insure that it could be reliable for the other region as well. Due to lack of time and resource this study was based on only an event which is the limitation of this research. Numerous study should be conducted to determine the model performance. So, additional research should be required using several event along with many more schemes to accurately and timely predict the events as well as to draw the general conclusion for the improvements of the operational forecasting. In addition, such type of research using WRF model has great importance in the complex topographical region like Nepal.

REFERENCES

A J, L., Mohanty, U.C., 2008. Simulation of a severe thunderstorm event during the field experiment of STORM programme 2006, using WRF-NMM model. Curr. Sci. 95, 204–215.

Adhikari, B.R., 2021. Lightning Fatalities and Injuries in Nepal. Weather Clim. Soc. 13, 449–458. https://doi.org/10.1175/WCAS-D-20-0106.1

Ahasan, M.N., Quadir, D.A., Khan, K.A., Haque, M.S., 2015. SIMULATION OF A THUNDERSTORM EVENT OVER BANGLADESH USING WRF-ARW MODEL. J. Mech. Eng. 44, 124–131. https://doi.org/10.3329/jme.v44i2.21437

Aryal, D., 2018. (PDF) Pre-Monsoon Thunderstorms in Nepal [WWW Document]. ResearchGate. https://doi.org/10.22161/ijreh.2.3.5

Bonekamp, P.N.J., Collier, E., Immerzeel, W.W., 2018. The Impact of Spatial Resolution, Land Use, and Spinup Time on Resolving Spatial Precipitation Patterns in the Himalayas. J. Hydrometeorol. 19, 1565–1581. https://doi.org/10.1175/JHM-D-17-0212.1

Carlson TN, Ludlum FH. 1968. Conditions for the occurrence of severe local storms. Tellus 20: 203–226.

Chevuturi, A., Dimri, A.P., 2015. Inter-comparison of physical processes associated with winter and non-winter hailstorms using the weather research and forecasting (WRF) model. Model. Earth Syst. Environ. 1, 9. https://doi.org/10.1007/s40808-015-0014-5

Chevuturi, A., Dimri, A.P., Gunturu, U.B., 2014. Numerical simulation of a rare winter hailstorm event over Delhi, India on 17 January 2013. Nat. Hazards Earth Syst. Sci. 14, 3331–3344. https://doi.org/10.5194/nhess-14-3331-2014

Chhetri, P.D.T.B., Dawadi, Dr.B.,Dhital, D.Y.P., 2019. Detection of a Tornado event on March31(2019) and its effects on the Eastern part of Nepal. Indian J. Sci. Technol. 12, 1–5. https://doi.org/10.17485/ijst/2019/v12i38/146311

Christian, H.J., Blakeslee, R.J., Boccippio, D.J., Boeck, W.L., Buechler, D.E., Driscoll, K.T., Goodman, S.J., Hall, J.M., Koshak, W.J., Mach, D.M., Stewart, M.F., 2003. Global frequency and distribution of lightning as observed from space by the Optical Transient Detector. J. Geophys. Res. 108.

Das, M.K., Das, S., Chowdhury, Md.A.M.,Karmakar, S., 2016. Simulation of tornado over Brahmanbaria on 22 March 2013 using Doppler weather radar and WRF model. Geomat. Nat. Hazards Risk 7, 1577–1599.https://doi.org/10.1080/19475705.2015.1115432

Dewan, A., Ongee, E.T., Rahman, Md.M.,Mahmood, R., Yamane, Y., 2018. Spatial and temporal analysis of a 17-year lightning climatology over Bangladesh with LIS data. Theor. Appl. Climatol. 134, 347–362. https://doi.org/10.1007/s00704-017-2278-3

Ferrier, B.S., 1994. A Double-Moment Multiple-Phase Four-Class Bulk Ice Scheme. Part I: Description. J. Atmospheric Sci. 51, 249–280. https://doi.org/10.1175/1520-0469(1994)051<0249:ADMMPF>2.0.CO;2

G., P.R., M., Rajasekhar, R., P.S., T., S., M., Rajeevan, Ramakrishna, S.S.V.S., 2016. Prediction of severe thunderstorms over Sriharikota Island by using the WRF-ARW operational model, in: Krishnamurti, T.N., Rajeevan, M.N. (Eds.), . Presented at the SPIE Asia-Pacific Remote Sensing, New Delhi, India, p. 988214. https://doi.org/10.1117/12.2225068

Islam, A.R.Md.T., Nafiuzzaman, Md., Rifat, J., Rahman, M.A., Chu, R., Li, M., 2020.

Karki, R., Hasson, S. ul, Gerlitz, L., Talchabhadel, R., Schenk, E., Schickhoff, U., Scholten, T., Böhner, J., 2018. WRF-based simulation of an extreme precipitation event over the Central Himalayas: Atmospheric mechanisms and their representation by microphysics parameterization schemes. Atmospheric Res. 214, 21–35. https://doi.org/10.1016/j.atmosres.2018.07.016

Kumar, M. S., Shekhar, M. S., Krishna, S. R., Bhutiyani, M. R., &Ganju, A. (2012). Numerical simulation of cloud burst event on August 05, 2010, over Leh using WRF mesoscale model. *Natural Hazards*, *62*(3), 1261–1271.

Laing, A. G. and J. M. Fritsch, 1993: Mesoscale convective complexes over the Indian monsoon region. *J. Climate*., **6**, 911-919.

Maddox, R.A., Chappell, C.F., Hoxit, L.R., 1979. Synoptic and Meso-α Scale Aspects of Flash Flood Events. Bull. Am. Meteorol. Soc. 60, 115–123. https://doi.org/10.1175/1520-0477-60.2.115

Mäkelä, A., Shrestha, R., Karki, R., 2012. Thunderstorm characteristics in Nepal during the pre-monsoon season 2012. Atmospheric Res. 137, 91–99.

Mandhar, G. K., S. S. Kandalgaonkar and M. I. R. Tinmaker, 1999: Thunderstorm activity over India and the Indian southwest monsoon. J. *Geophys. Rsch.*,104, 4169-4188.

Mannan, A., Ahasan, N., Alam, S., 2015. Study of Severe Thunderstorms over Bangladesh and Its Surrounding Areas During Pre-monsoon Season of 2013 Using WRF-ARW Model, in: Ray, K., Mohapatra, M., Bandyopadhyay, B.K., Rathore, L.S. (Eds.), High-Impact Weather Events over the SAARC Region. Springer International Publishing, Cham, pp. 3–22. https://doi.org/10.1007/978-3-319-10217-7_1

Manohar, G.K., Kesarkar, A.P., 2005. Climatology of thunderstorm activity over the Indian region : III. Latitudinal and seasonal variation 12.

Meteorol. Atmospheric Phys. 132, 793–808. https://doi.org/10.1007/s00703-019-00720-6

Meyer, J.D.D., Pokharel, B., Gillies, R.R., 2021. Simulating the storm environment responsible for Nepal's first observed tornado. Weather Clim. Extrem. 34, 100368. https://doi.org/10.1016/j.wace.2021.100368

Murthy, B.S., Latha, R., Madhuparna, H., 2018. WRF simulation of a severe hailstorm over Baramati: a study into the space–time evolution. Meteorol. Atmospheric Phys. 130, 153–167. https://doi.org/10.1007/s00703-017-0516-y

Norris, J., Carvalho, L.M.V., Jones, C., Cannon, F., Bookhagen, B., Palazzi, E., Tahir, A.A., 2017. The spatiotemporal variability of precipitation over the Himalaya: evaluation of one-year WRF model simulation. Clim. Dyn. 49, 2179–2204. https://doi.org/10.1007/s00382-016-3414-y

Orr, A., Listowski, C., Couttet, M., Collier, E., Immerzeel, W., Deb, P., & Bannister, D. (2017). Sensitivity of simulated summer monsoonal precipitation in Langtang Valley, Himalaya, to cloud microphysics schemes in WRF. *Journal of Geophysical Research: Atmospheres*, *122*(12), 6298–6318.

Pant, G. B., and K. Rupa Kumar, 1997: *Climates of South Asia*. John Wiley & Sons, New York, 320 pp.

Paul, P., Imran, A., Islam, J., Kabir, A., Jaman, S., Syed, I.M., n.d. Study of Pre-Monsoon Thunderstorms and Associated Thermodynamic Features Over Bangladesh Using WRF-ARW Model 6.

Rahman, M.M., Samad, M.A., Hassan, S.Q., 2018. Simulation of Thermodynamic Features of a Thunderstorm Event over Dhaka using WRF-ARW Model. GANIT J. Bangladesh Math. Soc. 37, 131–145. https://doi.org/10.3329/ganit.v37i0.35732

Rajeevan, M., Kesarkar, A., Thampi, S.B., Rao, T.N., Radhakrishna, B., Rajasekhar, M., 2010. Sensitivity of WRF cloud microphysics to simulations of a severe thunderstorm event over Southeast India. Ann. Geophys. 28, 603–619. https://doi.org/10.5194/angeo-28-603-2010

Rakesh, V., Singh, R., Joshi, P.C., 2009. Intercomparison of the performance of MM5/WRF with and without satellite data assimilation in short-range forecast applications over the Indian region. Meteorol. Atmospheric Phys. 105, 133–155. https://doi.org/10.1007/s00703-009-0038-3

Rao, Y. P., 1981: The Climate of the Indian Subcontinent. *World Survey of Climatology*, **9**, 67-182. Elsevier, Amsterdam.

Robinson, P.J., Henderson-Sellers, A., 1999. Contemporary climatology. Addison Wesley Longman, Singapore (317 pp.).

Saha, K., Damase, N.P., Banik, T., Paul, B., Sharma, S., De, B.K., Guha, A., 2019. Satellite-based observation of lightning climatology over Nepal. J. Earth Syst. Sci. 128, 221. https://doi.org/10.1007/s12040-019-1239-x

Sari, F.P., Baskoro, A.P., Hakim, O.S., 2018. Effect of different microphysics scheme on WRF model: A simulation of hail event study case in Surabaya, Indonesia. Presented at the INTERNATIONAL SYMPOSIUM ON EARTH HAZARD AND DISASTER MITIGATION (ISEDM) 2017: The 7th Annual Symposium on Earthquake and Related Geohazard Research for Disaster Risk Reduction, Bandung, Indonesia, p. 020002. https://doi.org/10.1063/1.5047287

Shrestha, R. K., Connolly, P. J., & Gallagher, M. W. (2017). Sensitivity of WRF cloud microphysics to simulations of a convective storm over the Nepal Himalayas. *The Open Atmospheric Science Journal*, *11*(1).

Singh, J., Das, S., Gairola, A., 2017. Study of Severe Thunderstorm Event on 30-31 May 2014 10.

Skamarock, W.C., Klemp, J.B., Dudhia, J., Gill, D.O., Liu, Z., Berner, J., Wang, W., Powers, J.G., Duda, M.G., Barker, D.M., Huang, X.-Y., 2019. A Description of the Advanced Research WRF Model Version 4 162. Spatiotemporal variations of thunderstorm frequency and its prediction over Bangladesh.

Suresh, R., 2012. Forecasting and nowcasting convective weather phenomena over southern peninsular india - part I: Thunderstorms. Indian J. Radio Space Phys. 41, 421–434.

Tajbakhsh, S., Ghafarian, P., Sahraian, F., 2012. Instability indices and forecasting thunderstorms: the case of 30 April 2009. Nat. Hazards Earth Syst. Sci. 12, 403–413. https://doi.org/10.5194/nhess-12-403-2012

Yamane, Y., Hayashi, T., Dewan, A.M., Akter, F., 2010. Severe local convective storms in Bangladesh: Part I. Climatology. Atmospheric Res. 95, 400–406. https://doi.org/10.1016/j.atmosres.2009.11.004

ANNEXES

Namelist WRF

```
&time_control
start_year                          = 2019,     2019,     2019,
start_month                         = 04,       04,      04,
start_day                           = 28,       28,       28,
start_hour                          = 12,       12,       12,
start_minute                        = 00,       00,       00,
start_second                        = 00,       00,       00,
end_year                            = 2019,     2019,     2019,
end_month                           = 04,       04,       04,
end_day                             = 30,       30,       30,
end_hour                            = 00,       00,       00,
end_minute                          = 00,       00,       00,
end_second                          = 00,       00,       00,
interval_seconds                    = 21600,
input_from_file                     = .true.,   .true.,   .true.,
history_interval                    = 30,       30,       30,
frames_per_outfile                  = 1000,     1000,     1000,
restart                             = .false.,
restart_interval                    = 2160,
io_form_history                     = 2,
io_form_restart                     = 2,
io_form_input                       = 2,
io_form_boundary                    = 2,
debug_level                         = 0,
/


&domains
time_step                           = 120,
time_step_fract_num                 = 0,
time_step_fract_den                 = 1,
max_dom                             = 3,
e_we                                = 130,      211,      446,
e_sn                                = 130,      156,      341,
e_vert                              = 35,       35,       35,
p_top_requested                     = 5000,
num_metgrid_levels                  = 32,
num_metgrid_soil_levels             = 4,
dx                                  = 25000,     5000,     1000,
dy                                  = 25000,     5000,     1000,
grid_id                             = 1,        2,        3,
parent_id                           = 1,        1,        2,
i_parent_start                      = 1,       53,       69,
j_parent_start                      = 1,       77,       44,
parent_grid_ratio                   = 1,        5,        5,
parent_time_step_ratio              = 1,        5,        5,
feedback                            = 1,
smooth_option                       = 0,
/

&physics
mp_physics                          = 8,        8,        8,
ra_lw_physics                       = 1,        1,        1,
ra_sw_physics                       = 1,        1,        1,
```

```
radt                                = 30,       30,       30,
sf_sfclay_physics                   = 1,        1,        1,
sf_surface_physics                  = 2,        2,        2,
bl_pbl_physics                      = 1,        1,        1,
bldt                                = 0,        0,        0,
cu_physics                          = 1,        1,        0,
cudt                                = 5,        5,        5,
isfflx                              = 1,
ifsnow                              = 0,
icloud                              = 1,
surface_input_source                = 1,
num_soil_layers                     = 4,
sf_urban_physics                    = 0,        0,        0,
maxiens                             = 1,
maxens                              = 3,
maxens2                             = 3,
maxens3                             = 16,
ensdim                              = 144,
/

&fdda
/

&dynamics
w_damping                           = 0,
diff_opt                            = 1,
km_opt                              = 4,
diff_6th_opt                        = 0,        0,        0,
diff_6th_factor                     = 0.12,     0.12,     0.12,
base_temp                           = 290.,
damp_opt                            = 0,
zdamp                               = 5000.,    5000.,    5000.,
dampcoef                            = 0.2,      0.2,      0.2,
khdif                               = 0,        0,        0,
kvdif                               = 0,        0,        0,
non_hydrostatic                     = .true.,   .true.,   .true.,
moist_adv_opt                       = 1,        1,        1,
scalar_adv_opt                      = 1,        1,        1,
/

&bdy_control
spec_bdy_width                      = 5,
spec_zone                           = 1,
relax_zone                          = 4,
specified                           = .true.,  .false.,  .false.,
nested                              = .false.,   .true.,   .true.,
/

&grib2
/

&namelist_quilt
nio_tasks_per_group                 = 0,
nio_groups                          = 1,
/
```

Namelist WPS

```
&share
 wrf_core = 'ARW',
 max_dom = 3,
 start_date = 2019-04-28_12:00:00, 2019-04-28_12:00:00, 2019-04-
28_12:00:00,
 end_date   = 2019-04-30_00:00:00, 2019-04-30_00:00:00, 2019-04-
30_00:00:00,
 interval_seconds = 21600,
 io_form_geogrid = 2,
 opt_output_from_geogrid_path =
'/NWP/krishna/pokhara_429/thompson1/wps' ,
 debug_level = 0,
/
&geogrid
 parent_id         = 1,1,2,
 parent_grid_ratio = 1,5,5,
 i_parent_start    = 1,53,69,
 j_parent_start    = 1,77,44,
 e_we          = 130,211,446,
 e_sn          = 130,156,341,
 geog_data_res = 'lowres','lowres','lowres',
 dx = 25000,
 dy = 25000,
 map_proj =  'mercator',
 ref_lat   = 22,
 ref_lon   = 82,
 truelat1  = 22,
 truelat2  = 0,
 stand_lon = 82,
 geog_data_path = '/NWP/WRFV4/geog/WPS_GEOG_LOW_RES',
 opt_geogrid_tbl_path = '/NWP/krishna/pokhara_429/thompson1/wps',
 ref_x = 65.0,
 ref_y = 65.0,
/

&ungrib
 out_format = 'WPS',
 prefix = 'FILE',
/

&metgrid
 fg_name = 'FILE',
 io_form_metgrid = 2,
 opt_output_from_metgrid_path =
'/NWP/krishna/pokhara_429/thompson1/wps',
 opt_metgrid_tbl_path = '/NWP/krishna/pokhara_429/thompson1/wps',
/

&mod_levs
 press_pa = 201300 , 200100 , 100000 ,
             95000 ,  90000 ,
             85000 ,  80000 ,
             75000 ,  70000 ,
             65000 ,  60000 ,
             55000 ,  50000 ,
             45000 ,  40000 ,
```

```
             35000 ,  30000 ,
             25000 ,  20000 ,
             15000 ,  10000 ,
              5000 ,   1000
 /


&domain_wizard
 grib_data_path = 'null',
 grib_vtable = 'null',
 dwiz_name    =abcdef
 dwiz_desc    =
 dwiz_user_rect_x1 =2811
 dwiz_user_rect_y1 =569
 dwiz_user_rect_x2 =3086
 dwiz_user_rect_y2 =961
 dwiz_show_political =true
 dwiz_center_over_gmt =true
 dwiz_latlon_space_in_deg =10
 dwiz_latlon_linecolor =-8355712
 dwiz_map_scale_pct =25.0
 dwiz_map_vert_scrollbar_pos =507
 dwiz_map_horiz_scrollbar_pos =2569
 dwiz_gridpt_dist_km =25.0
 dwiz_mpi_command =null
 dwiz_tcvitals =null
 dwiz_bigmap =Y
/
```